Capillary Effects in Fiber Reinforced Polymer Composite Processing: A Review

Helena Teixidó[1†], Jeroen Staal[1†], Baris Caglar[2] and Véronique Michaud[1*]

[1]Laboratory for Processing of Advanced Composites (LPAC), Institute of Materials (IMX), Ecole Polytechnique Fédérale de Lausanne (EPFL), Lausanne, Switzerland, [2]Aerospace Manufacturing Technologies, Faculty of Aerospace Engineering, Delft University of Technology, Delft, Netherlands

Capillarity plays a crucial role in many natural and engineered systems, ranging from nutrient delivery in plants to functional textiles for wear comfort or thermal heat pipes for heat dissipation. Unlike nano- or microfluidic systems with well-defined pore network geometries and well-understood capillary flow, fiber textiles or preforms used in composite structures exhibit highly anisotropic pore networks that span from micron scale pores between fibers to millimeter scale pores between fiber yarns that are woven or stitched into a textile preform. Owing to the nature of the composite manufacturing processes, capillary action taking place in the complex network is usually coupled with hydrodynamics as well as the (chemo) rheology of the polymer matrices; these phenomena are known to play a crucial role in producing high quality composites. Despite its importance, the role of capillary effects in composite processing largely remained overlooked. Their magnitude is indeed rather low as compared to hydrodynamic effects, and it is difficult to characterize them due to a lack of adequate monitoring techniques to capture the time and spatial scale on which the capillary effects take place. There is a renewed interest in this topic, due to a combination of increasing demand for high performance composites and recent advances in experimental techniques as well as numerical modeling methods. The present review covers the developments in the identification, measurement and exploitation of capillary effects in composite manufacturing. A special focus is placed on Liquid Composite Molding processes, where a dry stack is impregnated with a low viscosity thermoset resin mainly via in-plane flow, thus exacerbating the capillary effects within the anisotropic pore network of the reinforcements. Experimental techniques to investigate the capillary effects and their evolution from post-mortem analyses to *in-situ*/rapid techniques compatible with both translucent and non-translucent reinforcements are reviewed. Approaches to control and enhance the capillary effects for improving composite quality are then introduced. This is complemented by a survey of numerical techniques to incorporate capillary effects in process simulation, material characterization and by the remaining challenges in the study of capillary effects in composite manufacturing.

Keywords: capillary effects, composite processing, liquid composite molding, textile preforms, fiber reinforced polymers

1 INTRODUCTION

Capillary action is defined as the process whereby a fluid flows on a surface, thus displacing air or another immiscible phase present on this solid surface, under no external forces, simply due to the presence of intermolecular forces between the liquid and the solid surface. These forces arise from the presence of the liquid/air surface tension and the interfacial tension between the solid and the liquid phase. A pressure difference is thus created between the pressure in the air and that in the fluid phase, driving fluid flow at the interface between solid, liquid and generally air. For example, these effects help the fluid phase move up against gravity in a capillary tube that was initially filled with air, if the energy balance is favorable when replacing a solid-air interface by a solid-liquid interface. In a circular capillary tube, the capillary pressure drop, ΔP_γ, is written as:

$$\Delta P_\gamma = -\frac{2\sigma_{lv}\cos\theta}{r} \qquad (1)$$

where θ is the contact angle between the liquid interface and the tube, σ_{lv} is the surface tension between the fluid and the ambient atmosphere, and r is the radius of the tube. $\Delta P_\gamma > 0$ thus indicates a non-wetting system whereas $\Delta P_\gamma < 0$ indicates a wetting system. Capillary forces play an important role in many physical systems where a fluid invades a network of narrow spaces, ensuring fluid circulation in plants, in the lacrimal ducts, wicks, brushes and towels, heat pipes, fountain pens, and of course they are at the base of hydrogeology and groundwater flow (Bear, 1972; Freeze and Cherry, 1979).

These effects are also found in composite processing, wherever an activated liquid monomer or polymer flows into the initially dry porous network formed by the reinforcing fibers (or powders); they will thus act close to the impregnation flow front, or in regions that are partially impregnated. In most cases, the reinforcing fibers or filaments, which have a diameter in the order of 7–20 μm, are produced in the form of yarns, comprising several thousands of filaments, which are then combined by textile processes into mats, woven, knitted or braided fabrics, as well as non-crimp fabrics or polymer bound tapes. As a result, fiber textiles or preforms used in composite structures exhibit highly anisotropic, in general dual scale pore networks that span from micron scale pores between fibers to millimeter scale pores between fiber yarns (Michaud, 2021). Owing to the nature of the composite manufacturing processes, capillary action is usually coupled with hydrodynamics, since flow is driven by externally applied pressure, as well as with the (chemo)rheology of the polymer matrices; in addition, the matrix material in liquid form is generally much more viscous than water, up to several orders of magnitude, leading to a strong dependence of the mechanisms to the interface velocity. Despite their importance, capillary effects largely remained overlooked in composite processing research. Their magnitude is rather low as compared to hydrodynamic effects, which dominate the flow kinetics. In general, the capillary pressure values found in composite processing are in the range of 1–70 kPa, whereas applied pressures are in the range of 10^2–10^3 kPa. In addition, it is difficult to characterize them due to a lack of adequate monitoring techniques to capture the time and spatial scale on which the capillary effects take place, and to model them, as they require rather advanced fluid flow analysis and the knowledge of the physical phenomena taking place close to the flow front. Interest is nonetheless rapidly increasing, due to a gain in process maturity and thus higher demand for high performance, low porosity composites and to recent advances in experimental techniques as well as numerical modeling methods. The present review addresses these, with particular focus on Liquid Composite Molding (LCM) processes, where a dry fabric stack is impregnated with a low viscosity thermoset resin mainly via in-plane flow, thus exacerbating the capillary effects within the anisotropic pore network of the reinforcements.
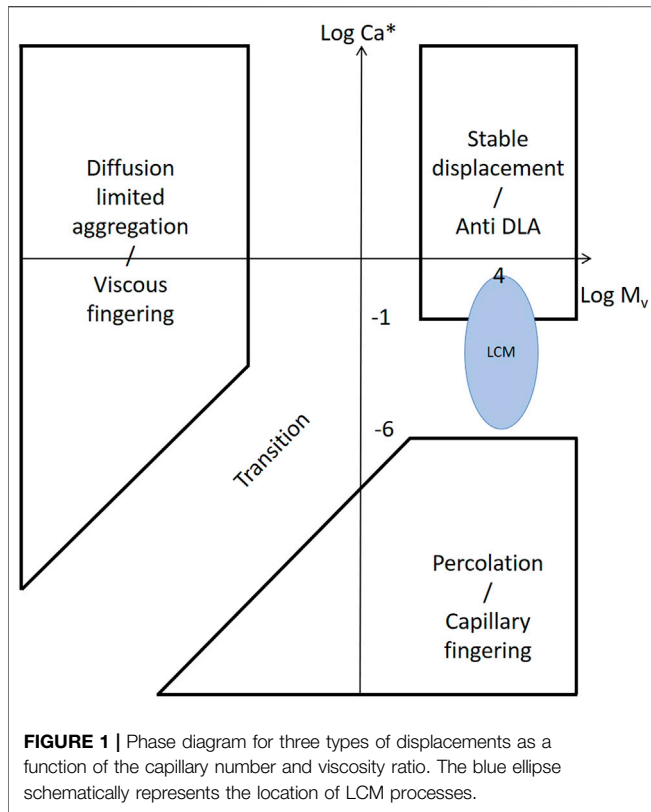
2 CAPILLARY EFFECTS IN POROUS MEDIA: PHYSICAL PRINCIPLES

Capillary effects in porous media are directly linked to the wetting of an initially dry porous medium by a fluid phase. Wetting is the ability of a liquid to stay in contact with a solid due to intermolecular interactions, creating a balance between adhesive and cohesive forces. The main parameters controlling capillary effects can be considered based on the different length scales they operate on, from the molecular scale controlling chemical and molecular interactions very close to the solid-liquid-air interface, to the sub-pore and pore scale where surface energy considerations lead to contact angles and menisci, up to the Representative Volume Element (RVE) scale, where macroscopic saturation is observed. The link between the thermodynamic and geometric considerations acting at these length scales has been the subject of intense work with many remaining open questions in the fields related to soil science, as recently reviewed by Armstrong et al. (Armstrong et al., 2021). Although we will consider thermodynamic effects and the possibility to modify the surface of the reinforcement to change wettability, we will mostly focus on the macroscopic or pore scale effects in this review, as these are most relevant in composite manufacturing, due to the presence of additional body forces beyond capillary forces.

As reviewed in Ref. (Michaud, 2016), the patterns found when a fluid displaces another one within a porous medium strongly depend on two parameters, which are the ratio of the invading (η_{resin}) to the displaced (η_{air}) fluid viscosity, $M_v = \frac{\eta_{resin}}{\eta_{air}}$, and the modified capillary number (as commonly referred to in literature on composite processing), a dimensionless number defined in soil science as:

$$Ca^* = \frac{Q}{A}\frac{\eta_{resin}}{\sigma_{lv}\cos\theta} \qquad (2)$$

where Q is the invading fluid flow rate, A the cross-sectional area of the porous medium. The value of these two parameters defines a range of infiltration front patterns, from percolation and capillary fingering to viscous fingering, as illustrated in **Figure 1** for the case of a rather homogeneous porous

FIGURE 1 | Phase diagram for three types of displacements as a function of the capillary number and viscosity ratio. The blue ellipse schematically represents the location of LCM processes.

medium. In cases typical of LCM, where the invading fluid has a much higher viscosity than the air present in the fibrous preform, M_v is large, and the flow regime can vary from capillary fingering for very low Ca^* to a stable, hydrodynamics dominated plug flow displacement for large Ca^*. Note that for fluids of rather high viscosity as generally found in matrices used in composite manufacturing, as the contact angle strongly depends on the fluid velocity, as will be discussed later, the capillary number is often simply taken as:

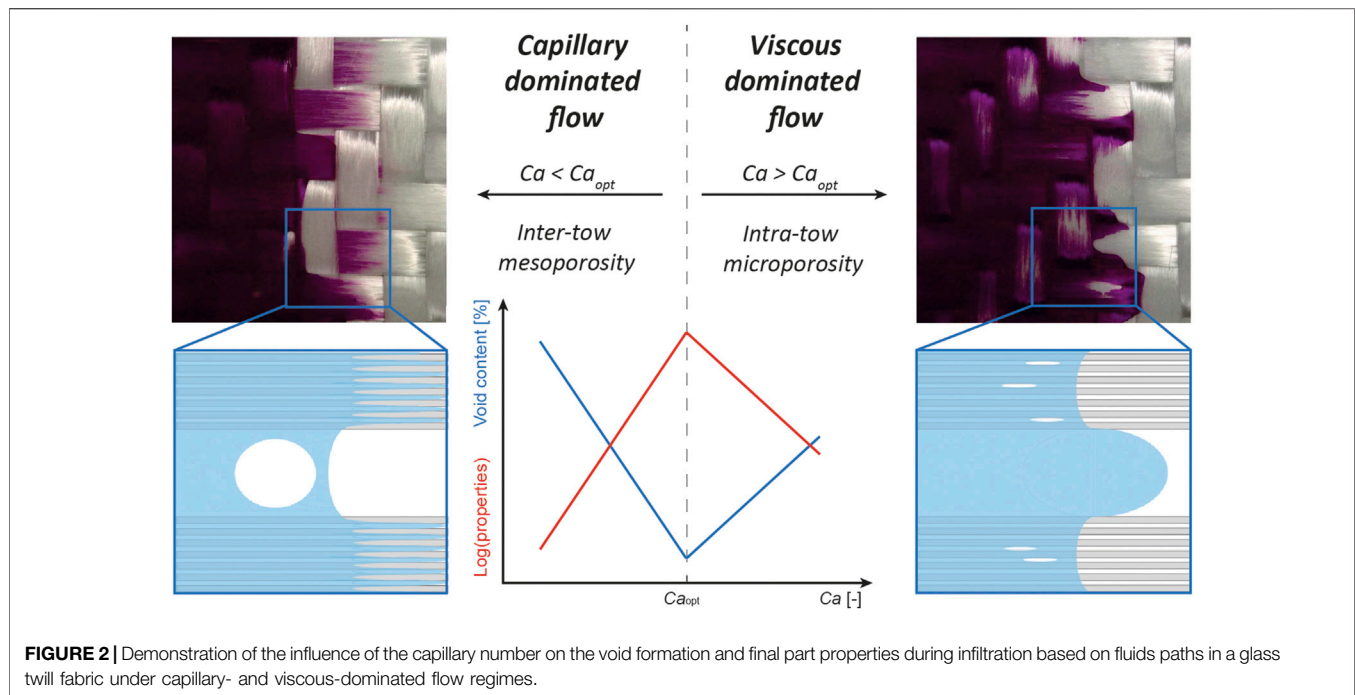$$Ca = \frac{Q}{A} \frac{\eta_{resin}}{\sigma_{lv}} \qquad (3)$$

In polymer composite processing, fingering and percolation effects are generally omitted, whereas this approach has been applied to metal matrix composite processing where these effects are observed (Michaud et al., 1994; Léger et al., 2014, Léger et al., 2015; Schneider et al., 2019; Varnavides et al., 2021). Most of the soil science (as well as metal matrix composites) analysis considers a rather homogeneous porous medium without the dual scale and highly localized pore structures observed in polymer composite processing, apart from cases of fractured rocks (Sahimi, 2011), which could be used as an inspiration to the pore network description of textiles. Even the fractured rocks are often considered to contain randomly distributed channels rather than well-organized structures, thus leaving the textiles as a particular case with anisotropic pore networks formed via large inter-tow regions and small intra-tow regions.

As mentioned previously, fibrous reinforcements used in advanced composites generally exhibit a bimodal pore

distribution. More specifically, pores present between the fibers in a yarn are referred to as micro-pores and empty space between the yarns are called meso-pores. Irrespective of the manufacturing process, an outcome of this pore characteristic is a matrix/fabric interaction at different scales that generally leads to a dual scale flow during resin infiltration (Bonnard et al., 2017). Hydrodynamic forces resulting from the applied pressure differential drive the impregnation process. However, the viscous drag is significantly higher in micro-pores (i.e., where permeability is lower). In addition, capillary forces are present at the fluid/fiber interface and the coupling between the yarn permeability, overall preform permeability and the capillary effects yield a complex relationship in terms of relative influence of flow within and between tows.

The interplay between different flow modes (micro- and meso-, viscous flow or capillary flow) results in formation of voids that change in shape and location depending on the extent of viscous and capillary driven flows. Void presence in an advanced composite is known to significantly reduce the mechanical performance of these materials and their formation as well as transport and removal has been studied in the literature (Lundström et al., 1993; Binetruy and Hilaire, 1998; Kang et al., 2000; Bréard et al., 2003b; Ruiz et al., 2006; Leclerc and Ruiz, 2008; Park et al., 2011; Abdelwahed et al., 2014; Gueroult et al., 2014; Mehdikhani et al., 2019; Castro et al., 2021). Despite the existence of several sources of void formation such as mechanical air entrapment, nucleation, leakage and cavitation; air entrapment is known to be the most common mechanism in LCM process, originating from the abovementioned dual scale porosity induced flow phenomena (Park and Lee, 2011; Mehdikhani et al., 2019). For a given system, higher Ca indicates dominance of viscous forces over capillary forces and vice versa. In the extremely slow impregnation situations with flow front speeds in the range of few mm/min, micro-flow progresses ahead of the meso-flow and results in entrapment of μm to mm sized spherical voids between tows (as illustrated in **Figure 2**). Similarly, high impregnation rates with typical flow front speeds in the range of several cm/min or higher, results in a delay of impregnation of small spaces between fibers in tows and in return causes formation of elliptically shaped, higher aspect ratio voids in the intra-tow spaces (Leclerc and Ruiz, 2008).

There exists a flow regime where the viscous and capillary forces are in balance which corresponds to an optimum capillary number, also referred to as Ca_{opt} (Leclerc and Ruiz, 2008; Park et al., 2011; LeBel et al., 2014). Void content as a function of Ca has been characterized experimentally (Leclerc and Ruiz, 2008) and numerically (Devalve and Pitchumani, 2013) and is known to follow a "V-shaped" trend as sketched in **Figure 2**. However the range of Ca_{opt} is known to differ for different matrix/fabric systems and as reported by Park (Park and Lee, 2011) and by Michaud (Michaud, 2016), typical values range in the order of 10–3 and in recent studies of Caglar et al. (Caglar et al., 2019) found a value of $1.4 \cdot 10^{-3}$, Lebel et al. (LeBel et al., 2019) a value of $1.5 \cdot 10^{-3}$ and Lystrup et al. (Lystrup et al., 2021) a value of $0.6 \cdot 10^{-3}$. The soil science version of the capillary number (Ca^*), as written

FIGURE 2 | Demonstration of the influence of the capillary number on the void formation and final part properties during infiltration based on fluids paths in a glass twill fabric under capillary- and viscous-dominated flow regimes.

in **Eq. 2**, is preferred in some studies, introducing the static contact angle between the matrix and fibrous reinforcement (θ_0) (Ruiz et al., 2006; Ravey et al., 2014; LeBel et al., 2017).

Alternative approaches have also taken place towards the definition of other non-dimensional numbers as an alternative to Ca and their use for identifying the optimal processing conditions, as the so-called Ca_{opt} is merely an intrinsic property of the matrix/fabric system and does not consider the process history (such as spatiotemporal variation of pressure and the formation and transport of voids as a result). Lawrence et al. (Lawrence et al., 2009) and Facciotto et al. (Facciotto et al., 2021) opted for using the so-called capillary ratio ($C = \Delta P_\gamma / P_{inj}$) to account for the changes in the flow velocity over time. Lebel et al. (LeBel et al., 2019) defined a critical capillary number that is required to mobilize a void. In a similar vein, Matsuzaki et al. (Matsuzaki et al., 2015) developed an analytical expression to predict the void formation in anisotropic woven fabrics by decoupling the flow in different domains (meso-flow, transverse and axial micro-flow) and defining criteria for void formation depending on the relation between the required times to fill each domain.

Determination of Ca_{opt} or its modified counterpart (Ca^*_{opt}), as well as the other non-dimensional numbers discussed so far heavily relies on experimental studies with limitations that will be highlighted in the next section, as the current state of research is still far from linking the process conditions and geometrical descriptions of arbitrary matrix/fabric systems to a Ca_{opt} without requiring laborious experiments. Despite the efforts towards achieving flow simulation with ever increasing accuracy and fidelity, the complexity of the underlying physics and the need to account for those at several length scales hinders the developments in the field. The following sections will provide

an overview of current developments in the experimental approaches for characterizing the extent of capillary effects in composite manufacturing and their link with residual porosity. Conventional approaches such as post-mortem analysis of composites will be followed by a survey of more advanced methods suitable for translucent reinforcements, mostly glass fibers, and recent developments in experimental approaches to study the capillary phenomena in other types of reinforcements, including but not limited to carbon fibers and natural fibers. Subsequent sections will then present the modeling efforts starting from microscale models to multiscale models that are inspired from the soil science literature to dual-scale models implemented using different numerical solvers and to semi-analytical approaches proposed to overcome the limitations of Ca-based residual void prediction.

3 OBSERVATION OF CAPILLARY EFFECTS

3.1 Capillary Wicking

Capillary pressure can be characterized in capillary wicking experiments, allowing for direct quantification from a single experiment. Amico and Lekakou (Amico and Lekakou, 2002) proposed a methodology where a fiber bundle, or a single ply of fibrous reinforcement (Caglar et al., 2019), is partially immersed into a probe liquid, where the capillary pressure was directly derived from the rate of weight gain or height increase. Pucci et al. (Pucci et al., 2015b) proposed a tensiometric method, based on Washburn's method (Washburn, 1921), to characterize capillary wicking of water and n-hexane in stacks of carbon fibrous preforms. By varying the orientation of the fibrous preforms they were able to determine the advancing contact angles in three,

i.e., weft, warp and through-thickness, directions, from which equivalent capillary pressures were derived. With coefficients of variation in the order of 30% this methodology is expected to be less accurate than that proposed by Amico and Lekakou (Amico and Lekakou, 2002) but the possibility to characterize fabric stacks and potentially vary fiber volume fractions makes it a very suitable method to apply in the context of LCM processing. It should be noted that capillary pressures measured in capillary wicking tests are not directly representative of those acting in LCM processes as the typical fluid velocities (hence *Ca*) encountered in these processes are not reached, in contrast to, e.g., direct flow experiments under a given applied pressure or flow rate (Salvatori et al., 2018). Nonetheless, capillary wicking experiments can be a valuable tool to obtain a first indication of capillary pressure in fibrous reinforcements, and to test changes in fiber surface conditions, volume fraction or pore morphology.

3.2 Post-Mortem Analysis

Post-mortem analysis on produced composite parts was the first and a facile method to observe and quantify the role of capillary effects. Post-mortem methods almost uniquely quantify capillary effects via the void content present after final consolidation of the composite, while varying process parameters (Lundström et al., 1993; Lundström and Gebart, 1994; Patel and Lee, 1995; Patel and Lee, 1996; Labat et al., 2001a; Leclerc and Ruiz, 2008) such as the flow rate or injection pressure and thereby the impregnation velocity. It is important to note that for impregnation under constant applied pressure, the velocity of the flow front decreases with the impregnation length. The presence of an optimum *Ca* (Patel and Lee, 1995; Patel and Lee, 1996; Labat et al., 2001a; Leclerc and Ruiz, 2008), where minimum void content is present within the composite, was often reported, while similar consequential observations were made for the resulting tensile modulus and tensile strength (Leclerc and Ruiz, 2008). While bringing the advantage of being an easy method with low equipment costs, post-mortem analysis of capillary effects could lead to large inaccuracies. These arise partially from the methods used for void content analysis such as, in order of increasing accuracy (Little et al., 2012), Archimedes (Kedari et al., 2011), microscopy (Lundström et al., 1993; Lundström and Gebart, 1994; Kedari et al., 2011) and micro-CT (Madra et al., 2014; Sisodia et al., 2016) methods, while part void content is also affected by phenomena occurring after passing of the flow front, e.g., void transport and dissolution into the resin. In spite of the strong assumption that part saturation in a chosen location does not change after passing of the flow front and during the cure/solidification process, these analyses have nonetheless been crucial to highlight the strong influence of capillary effects on part void content, as illustrated in **Figure 2**.

3.3 *In-situ* Analysis

An a priori more accurate method to analyze capillary effects taking place at the flow front is to observe, *in-situ*, the flow front progression and morphology, either very locally at the scale of a few fiber tows, or through the macroscopic analysis of the progressive saturation of the porous medium with the flowing fluid. These analy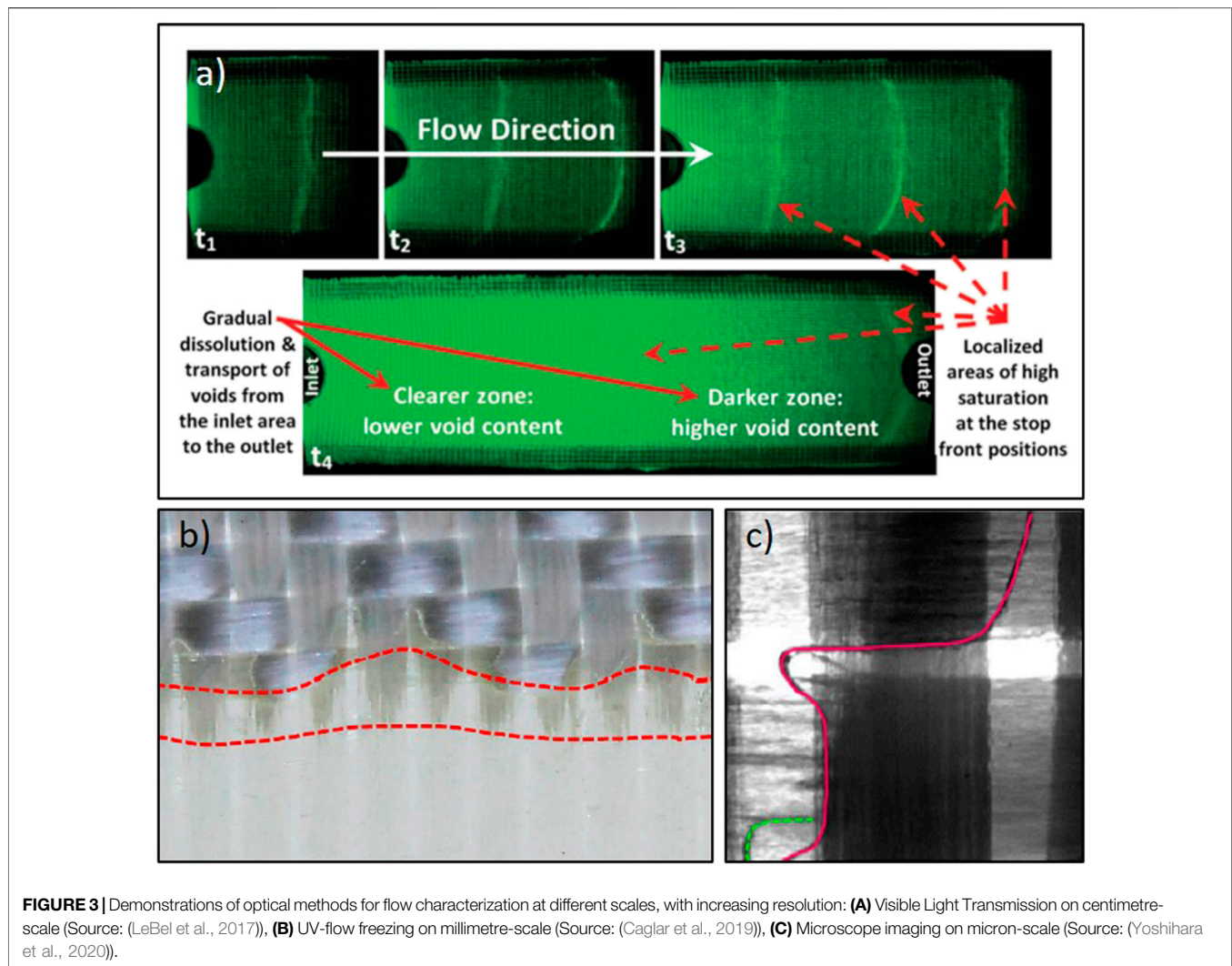ses usually refer to a saturation term, *S*, which is defined as the ratio of the volume fraction of liquid over the available pore space and is equal to 1 when the porous medium is fully filled with the liquid phase.

3.3.1 Transparent Fiber Reinforced Polymers

In-situ measurements allow for direct observations of capillary effects taking place in polymer composite processing. Optical methods can record impregnating resins in fibrous preforms in a non-intrusive manner and at a high spatial and time resolution with simple equipment, making it an effective and low-cost method for flow characterization (LeBel et al., 2019). Optical imaging is generally limited to translucent fabrics and relies on the matching of refractive indices to distinct phases (Lawrence et al., 2009; Nordlund and Michaud, 2012; LeBel et al., 2019), i.e., refractive indices of epoxy/fiberglass can be very different from that of the air/fiberglass interface and the distinction between the two interfaces can be further enhanced by colorants compatible with the test fluid (Caglar et al., 2018; Salvatori et al., 2018). Recording a linear flow with a conventional camera and subsequent image analysis has allowed Nordlund and Michaud (Nordlund and Michaud, 2012) and Facciotto et al. (Facciotto et al., 2021) to estimate the width of the unsaturated region, which was subsequently modelled with finite difference (Nordlund and Michaud, 2012) and finite element models (Facciotto et al., 2021). Continuous imaging of these regions showed the progressive saturation of the preform, which was quantified from the pixel intensity in the successive pictures. Standard camera imaging however only captures the flow at the surfaces of the mold (in general a glass top surface), which are known to be vulnerable to wall-effects, i.e., race-tracking between the preform and the mold halves, while effects such as nesting are also not well captured (Chen and Chou, 2000; Yousaf et al., 2017).

Visible Light Transmission (VLT), illustrated in **Figure 3A**, has been proposed as an elegant method to overcome this limitation (Lawrence et al., 2009). Placement of a diffuse light source below the transparent mold halves and of a camera above it makes the recorded light intensity an average over the preform thickness. Moreover, the signal is also significantly intensified. Lebel et al. (LeBel et al., 2017; LeBel et al., 2019) employed VLT to characterize the relation between processing conditions, i.e., *Ca**, and saturation of a glass fabric. The increased light intensity allowed them to accurately estimate the local void content after calibration with burn-off composites after consolidation. Distinction of voids allowed them to estimate the optimum *Ca** as well as the onset of pressure-induced void mobility. Further contrast enhancement could be achieved by the addition of fluorophores into the probe liquid. This resulted in strong contrast enhancement, e.g., for visualization of intratow flow (Lebel et al., 2013; LeBel et al., 2014), even enabling the use of optical methods in opaque carbon fibrous preforms (Lystrup et al., 2021). The addition of dyes may however induce changes in resin properties, e.g., wettability, and thereby may affect the apparent *Ca* or *Ca**, making the resulting observations not directly representative of pure resin systems.

Increases in spatial resolution and observations on tow-scale could be achieved with the use of optical microscopy imaging.

FIGURE 3 | Demonstrations of optical methods for flow characterization at different scales, with increasing resolution: **(A)** Visible Light Transmission on centimetre-scale (Source: (LeBel et al., 2017)), **(B)** UV-flow freezing on millimetre-scale (Source: (Caglar et al., 2019)), **(C)** Microscope imaging on micron-scale (Source: (Yoshihara et al., 2020)).

This increased resolution, however, comes at the cost of the overall field of view, making the method better suited for local detection of voids rather than for the assessment of saturation. Yoshihara et al. (Yoshihara et al., 2020) investigated the role of capillary pressure, varied by the application of different fluorine coatings on the fiber surface, on the dual-scale flow behavior in an optical microscopy setup. This allowed them to observe infusion of a woven fabric on a micron-scale, shown in **Figure 3C**, which were coupled to numerical simulations. Zhao et al. (Zhao et al., 2019) and Matsuzaki et al. (Matsuzaki et al., 2014) followed a similar approach in their studies on void formation and were able to accurately record capillary fingering and void formation upon the impregnation of a woven preform at a range of velocities falling in the capillary-dominated regime. This allowed them to accurately capture the void formation and evolution with the use of in-situ optical microscopy. However, flow analysis by means of optical microscopy can typically be applied to single ply fibrous reinforcements if based on light diffusion and suffers from the aforementioned wall effects in reflectance mode, while the upper limit of allowed infusion rates is defined by the maximum

imaging rate of the microscope. Caglar et al. (Caglar et al., 2019) proposed an in-situ UV flow-freezing method (**Figure 3B**), where infiltrating flows are in-situ cured by UV-photopolymerization. This overcomes any constraints in time resolution allowing for visualization of a large range of flow regimes. This method however requires the use of specially designed resin systems and rather thin and transparent samples to avoid inhibiting the cure reaction that is highly dependent on the penetration of UV light.

3.3.2 Non-Transparent Fiber Reinforced Polymers

The opaque nature of many commercially available fibers in polymer composites, e.g., carbon or flax, limits the optical observations of capillary effects in processing to the outer layers, which are susceptible to wall effects as discussed in **Section 3.3.1**. A multitude of methods have been proposed to overcome this limitation, ranging from methods already widely established in other fields, e.g., Magnetic Resonance Imaging (MRI), to more exploratory techniques such as infrared thermography. With no universal agreement on the preferred

technique to elucidate the degree of fluid saturation as a function of time and position, each specific method brings its own advantages and trade-offs between spatial resolution, recording speed and ease of implementation.

One of the proposed methods to track resin front progression and thereby indirectly record progressive saturation and void formation in LCM processing is the inclusion of sensors in or in-between stacked preforms (Konstantopoulos et al., 2014). Methods using conductive sensors typically require a non-conductive fibrous preform to be placed in between two conductive parallel plates. Labat et al. (Labat et al., 2001b) and later Gueroult et al. (Gueroult et al., 2014) infused a glass fiber preform with a conductive liquid and simultaneously recorded the voltage over the preform, which increased with increasing saturation. The first strong increase of the voltage was attributed to the passing of the unsaturated flow front followed by a period of void removal, while the final voltage was directly linked to the saturation and hence the void content in the part. The recorded void contents moreover followed the expected "V-shaped" curve as a function of Ca^*. Carlone et al. (Carlone and Palazzo, 2015; Carlone et al., 2018) employed a similar experimental methodology while recording the capacitance over the fabric preforms and correlated the observations to numerical models. This methodology also allowed for impregnation with less conductive resins. Similar saturation curves were obtained and verified in comparison with the void contents in post-mortem optical microscopy images. They moreover compared the accuracy of progressive saturation tracking by dielectric sensors with that recorded by pressure sensors, e.g., as proposed by Refs. (Di Fratta et al., 2013; Chiu et al., 2018), which was found to be significantly higher. The requirement for a non-conductive fibrous preform limits the use of the methods developed by Refs (Labat et al., 2001b; Gueroult et al., 2014; Carlone and Palazzo, 2015; Carlone et al., 2018). with several conventional fabric types. Developments have been made to overcome this issue, e.g., by insulating the sensor with a dielectric material and optimization of the sensor characteristics (Pouchias et al., 2019; Caglar et al., 2021a). However, these types of sensors have not yet been employed to study unsaturated flow phenomena to-date. Alternatively, Villière et al. (Villière et al., 2015) proposed a method based on the saturation-dependence of the thermal behavior of a resin-fiber system. Recording of heat fluxes induced by an electric heater was found to give an accurate representation of the local saturation, which were coupled with mathematical models to fit progressive saturation curves. Implementation of optical micro-flow sensors within tows on the other hand gives the possibility to record capillary pressures, as was demonstrated by He et al. (He et al., 2019) in their study on resin flow in prepreg processing. However, introducing thermal gradients in the fluid induces changes in the viscosity and surface tension characteristics and requires elaborated material characterization next to the experimental analyses.

The discrete nature of sensors limits the observations that can be made in a single impregnation while the spatial resolution of methods making use of integrated sensors is relatively low. Imaging techniques typically possess higher spatial resolution

over a larger section of the composite part. Ultrasound techniques are known for their high acquisition rates and have been used to track resin flow in fibrous preforms (Schmachtenberg et al., 2005), in particular for through-thickness resin infusion (Stöven et al., 2003; Thomas et al., 2008; Konstantopoulos et al., 2018). Thomas et al. (Thomas et al., 2008) tracked through-thickness resin flow via acoustic C-scan measurements giving a planar view of the sample. While this method gives an indication of through-thickness saturation of the preform, the limited spatial resolution does not allow for distinction of capillary effects such as localized saturation and void formation. Unsaturated permeability on the other hand was successfully characterized with use of ultrasound, given a microstructure-dependent minimum fiber content is present within the preform (Konstantopoulos et al., 2018).

Magnetic Resonance Imaging (MRI) (Callaghan, 1993) has been investigated as well to observe flow in porous media. While suffering from drawbacks such as large tooling costs and spatial resolutions that are limited to around 0.1 mm due to signal relaxation effects (Endruweit et al., 2011), MRI brings the advantage of an excellent material contrast between constituents of composites, i.e., fibers, polymer and voids, which could be further enhanced by the addition of contrasting agents or by specified measurement sequences (Neacsu et al., 2007). MRI has therefore been used for the characterization of flow in fibrous preforms (Mantle et al., 2001; Bijeljic et al., 2004; Bencsik et al., 2008), with several studies specifically focused on visualizing dual-scale flow behavior. Leisen and Beckham (Leisen and Beckham, 2008) proposed a method of nuclear MRI and subsequent image analysis to quantify inter-yarn voids and their morphologies in saturated woven nylon fabrics, while Neacsu et al. (Neacsu et al., 2007) applied MRI to characterize capillary effects in glass fiber bundles. In the latter case they found fast MRI imaging able to track progressive transversal impregnation within bundles with different volume fractions and were able to use this data to back calculate the driving capillary pressures. Endruweit et al. (Endruweit et al., 2011) carried out an extensive investigation regarding the use of MRI to in-situ image the impregnation of dual-scale textiles. Reconstructed 3D images had resolutions of 0.5 mm, visualizing the meso-structure of fibrous preforms. An intermittent injection strategy was used to overcome time resolution limitations, which allowed for imaging of various flow regimes. Resulting images clearly visualized the progressing flow front and the formation of inter-yarn voids, while progressive saturation was tracked by a gradual increase of relative signal intensities.

Intrinsic differences in X-ray absorption coefficients of composite constituents gave rise to a multitude of X-ray-based techniques that were applied to study in-situ the role of capillary effects in LCM processing. Bréard et al. (Bréard et al., 1999) continuously tracked through-thickness impregnation of a random mat stack using X-ray radiography. While image resolution was insufficient to capture the fibrous preform, fast imaging allowed for accurate tracking of the infiltrating fluids. Teixidó et al. (Teixidó et al., 2021) used an X-ray phase contrast method in-operando to assess saturation of several types of

fibrous preforms. Based on the material-sensitive phase modulation due to interference formed after passing X-rays through a grating, the material contrast, which can be a limiting factor for composites, is significantly enhanced (Gresil et al., 2017). Employing this method allowed them to image progressive saturation of 15 cm × 5 cm non-transparent fabrics over a range of capillary numbers and they were able to extract the thickness-averaged saturation curves from these images, with a time step below 10 s.

The use of X-ray micro computed tomography (µCT) has allowed for the observation of dual-scale flow at an unprecedented resolution. Based on the reconstruction of 3D images from a set of radial X-ray radiographs, X-ray µCT provides the ability to reconstruct through-thickness images of opaque materials (Withers et al., 2021). Features down to sub-µm can be reached, e.g., allowing for accurate imaging of carbon composites and of the void morphology, while image resolutions typically come at a cost of the volume that can be analyzed, and the measurement speed. 4D µCT imaging (3D in space and time), e.g., to study the dual-scale flow behavior, is moreover typically complicated by possible blurring effects occurring, reducing image resolution due to movement of the flow front (Castro et al., 2021). To avoid this, the acquisition time should be short enough to limit the movement to less than 1 voxel per scan (Castro et al., 2021). While some studies have thus aimed at indirect observations of dual-scale flow behavior, e.g., by assessing thickness changes (Hemmer et al., 2018) or image-based computational fluid dynamics simulations (Ali et al., 2019), several investigations aimed at in-situ imaging dual-scale flow behavior through a fibrous preform. Vilà et al. (Vilà et al., 2015) were the first to use µCT to study the intra-tow infiltration of a glass fiber bundle in a µCT synchrotron beamline. Infusion was carried out under a capillary-dominated regime and was halted to image the flow front. Images were reconstructed from 900 radiographs taken over a period of 120 min with a voxel size of 2.5 µm^3. At a slightly reduced resolution, Larson et al. (Larson and Zok, 2018; Larson et al., 2019) were able to drastically reduce the imaging time, i.e., to 1.5 min, which allowed them to in-situ record impregnation of an enclosed fiber bundle with capillary numbers up to 10^{-3}. They furthermore employed advanced segmentation methods to distinguish local saturated and dry sections. Vilà et al. (Vilà et al., 2015) and Larson et al. (Larson and Zok, 2018; Larson et al., 2019) were both able to observe progressive saturation of the fiber bundle and were able to relate this to local capillary pressures and permeabilities, while the more homogeneous fiber distributions of Larson et al. (Larson and Zok, 2018; Larson et al., 2019) resulted in more homogeneous distributions and magnitudes. They were moreover able to gain insight in the apparent dynamic contact angles and to relate this to fiber displacement. Static contact angles after capillary wicking of a fiber bundle was studied in more detail by Castro et al. (Castro et al., 2020), who employed synchrotron-µCT to produce high resolution images. Image analysis then allowed for an assessment of axial and transverse contact angles.

The resolution requirement to obtain an accurate representation of (carbon) composites with a conventional µCT setup limits the sample size significantly. Castro et al.

(Castro et al., 2021) overcame this limitation by making use of so-called synchrotron radiation computed laminography, where significant gains in field of view can be achieved by imaging planar samples at an angle (Helfen et al., 2011; Bull et al., 2013; Fisher et al., 2019). In combination with a fast acquisition rate, i.e., 1.8 min per tomogram, they were the first to in-situ image dual-scale flow behavior in woven textiles with micron-scale resolution. Equilibrated flow regimes (**Figure 4A**) were imaged and, although slightly affected by blurring due to movement of the flow front, the images clearly showed the microstructural evolution upon impregnation and the absence of void formation. Slower infusion rates in capillary-dominated regimes (**Figure 4B**) minimized the blurring effect, giving a highly detailed insight on progressive saturation and void formation upon impregnation. Moreover, they were able to segment and analyze both inter- and intra-yarn void distributions as well as gaining novel insights in the void formation mechanisms during LCM.

3.4 The Case of Natural Fiber Reinforced Polymers

Composites made of natural fibers, in general plant-based, are gaining interest for the development of more sustainable and eco-friendly composite materials. Natural fiber reinforced composites still present a large amount of porosity and processing defects mainly due an incomplete understanding of the role of the initial humidity level in the fibers, surface characteristics, depending on the fiber treatment such as alkali treatments, and their complex morphology (illustrated in **Figure 5**). Compared to synthetic fibers, plant based fibers are also known to suffer from extensive resin absorption and swelling due to their microstructure, which highly alter flow characteristics (Francucci et al., 2010; Pucci et al., 2017b; Garat et al., 2020; Salokhe et al., 2021). Moreover, they present irregular and complex morphological and surface properties. Fibers are built-up from elementary cells with a given length and an irregular cross-section, and are composed of a hierarchical sequence of wall layers of different composition and thicknesses around an internal closed cavity called the lumen (Pantaloni et al., 2021). Depending on the extraction conditions, fibers can be present in the fabric as elementary fibers with diameters around 20–40 µm or technical fibers (several elementary fibers bonded together with the middle lamella which acts as matrix) with larger variable sizes in the order of some hundred micrometers (Melelli et al., 2020). The fiber surface roughness together with the composition of lignin, cellulose and hemi-cellulose of the outer layer define the wetting properties of the natural fiber. Given the complexity of the porous network and surface properties of natural reinforcements, the understanding of infiltration and in particular of capillary effects has remained as a very complex issue to-date.

Dual-scale flow behavior and void formation mechanisms in LCM processes have also been observed in the case of natural fiber preforms (Pantaloni et al., 2020), and have received increasing attention over the past decade. Francucci et al. (Francucci et al., 2010) found that natural fibers exhibit capillary pressures that are two or three times higher

FIGURE 4 | Progressive saturation recorded by synchrotron radiation computed laminography of **(A)** Equilibrated and **(B)** Capillary dominated flow regimes (Source: (Castro et al., 2021)).

FIGURE 5 | Structure of natural fibers: Schematic representations of **(A)** technical (fiber bundle from the stem) and **(B)** elementary fiber, **(C)** optical microscopy image of technical and elementary fibers in a composite and **(D)** optical microscopy image of an elementary fiber surface.

compared to synthetic fibers, elucidating the relevance of micro-flows and capillary effects occurring during impregnation. Some authors attributed this to the hollow structure of the fibers (Francucci et al., 2010; Yin et al., 2018) however recent studies have shown limited evidence that the resin can impregnate the lumen since it is a closed cavity (Pantaloni et al., 2020). Due to the polar nature of the fibers, the model fluid chosen to carry impregnation measurements highly influences the study of capillary effects. For example, Francucci et al. (Francucci et al., 2010) carried out unidirectional impregnation experiments of woven jute fabrics with a water/glycerin solution and a vinylester resin. They measured the capillary pressure and obtained -25 and 36 kPa with the water-based solution and the resin respectively.

As already said, natural fibers are sensitive to liquid absorption. In consequence, during infiltration, fibers remove liquid from the main stream of infiltrating resin, acting as a sink component, decreasing the velocity of the flow as the fiber cross-section tends to enlarge due to liquid absorption and reduction in permeability during impregnation (Francucci et al., 2010; Testoni et al., 2018). Testoni et al. (Testoni et al., 2018) showed in capillary wicking tests that the swelling of the fibers leads to a reduction of the inter-fiber pores and thus an increase of the capillary pressure. With the aim of predicting and modeling the relation between capillarity and swelling in natural fibers, researchers used a similar approach based on physical wicking experiments coupled to modified Washburn's equations (Pucci et al., 2015a, 2016; Testoni et al., 2018; Vo et al., 2020). In wicking tests, synthetic fibers show a linear trend following Washburn's equation whereas a non-linear trend is usually observed for natural fibers due to swelling. Pucci et al. (Pucci et al., 2016) proposed a modified Washburn's equation, taking into account the change in the porosity due to swelling over time. They assumed a capillary radius decreasing linearly with time, from the initial to the final swollen values, when wicking the fabrics in water. More recently, Vo et al. (Vo et al., 2020) improved their numerical model by defining a dual scale porosity (dual scale capillary radius) of the flax fibers since wicking takes place in between individual yarns and in between elementary fibers. Swelling induced changes in the pore distribution and the effects on the capillary action more complex at high fiber volume fraction (V_f). The proposed method successfully predicted swelling of a flax fabric in water for V_f ranging from 30 to 60%. As recently reviewed by Pantaloni (Pantaloni et al., 2020), flow modelling taking into account both swelling and fluid absorption by the natural fibers could be carried out by modifying the continuity equation accordingly, allowing for changes in both saturation (through a sink term) and porosity over time.

3.5 Role of Sizing and Additional Phases in the Textile Preform

3.5.1 Role of the Fiber Surface Treatment

Commercial fibrous preforms are coated with sizings that form an interphase region between fibers and polymer (Thomason, 2021). Sizings are generally functionalized for compatibility with specific monomer types. Alteration of the surface chemistry of the fiber affects its wettability and thereby the capillary pressures exerted on infiltrating resins, in particular during intra-yarn flow (Palmese and Karbhari, 1995; Thomason, 2021). The wettability of commercial sizings is reported to vary strongly (Bernet et al., 2000) due to differences in the sizing composition, e.g., resin-fiber interactions of glass fibers determining contact angles are sensitive to the silane types (Wei et al., 1993; Araujo et al., 1995) and content present in the sizing (Nishioka, 1990; Karbhari and Palmese, 1997). Hence, the sizing composition could potentially be employed to control local capillary pressures and thereby dual-scale flow in LCM processing, but the confidential nature of commercial sizing compositions has impeded further investigations into the role of sizing compositions on the (intra-yarn) flow behavior. Sharma et al. (Sharma et al., 2009) observed that permeabilities of fibrous preforms, measured with silicon oil and Karo syrup as model fluid phases, are lower in the presence of a compatible sizing. In the absence of capillary effects, saturated permeability decreases due to the stronger resin-fiber interactions experienced by an infiltrating resin in the presence of a dedicated sizing. The decrease in capillary driven unsaturated flow was in agreement with the intra-yarn flow analysis as reported by Wang et al. (Wang et al., 2006) or Palmese and Karbhari (Palmese and Karbhari, 1995; Karbhari and Palmese, 1997) and was attributed to resin-fiber interactions to differences specific surface free energy (Steenkamer et al., 1995; Karbhari and Palmese, 1997). Capillary pressures moreover are reported to be lower for dedicated sizings due to the consequent increase of the contact angle. It should be noted however that dynamic, advancing, contact angles and thereby capillary pressures are highly dependent on the imposed flow rates in LCM (Karbhari and Palmese, 1997), which could potentially explain the decrease in capillary pressure in the presence of a dedicated sizing by increased induced wicking rates.

Surface treatments on sized fabrics have furthermore shown promise to control resin-fiber interactions in LCM processing. Physical treatments comprise electric discharge/plasma treatments, which are extensively employed in polymer composite production (Mittal et al., 2018). Application of electric discharge treatments increases polarity of the fiber surface due to the suggested formation of additional carboxyl and hydroxyl groups (Morent et al., 2008; Sinha and Panigrahi, 2009; Mittal et al., 2018). Caglar et al. (Caglar et al., 2019) assessed the influence of these oxidative treatments on the impregnation of glass fiber textiles. They found that the increased polarity decreased the capillary pressure drop, which subsequently accelerated capillary wicking. Analysis of UV-frozen flow fronts showed that the optimum Ca shifted after applying the treatment while the unsaturated region in capillary-dominated flow counterintuitively became smaller. This latter was attributed to a more favorable transverse flow when treated, spreading out the flow front. Application of this surface treatment strongly accelerated impregnation in capillary-dominated regimes, i.e., up to 50%. Further control of surface properties could be achieved by the application of numerous chemical treatments (Mittal et al., 2018). As an example, Yoshihara et al. (Yoshihara et al., 2020) controlled the capillary pressure

by the application of fluorine coatings on glass fiber textiles, which enhanced the capillary effects acting during resin infiltration.

3.5.2 Role of Additional Phases in the Textile Preform

In the search to expand the areas of use of polymer composites, strategies to introduce additional functions have been proposed. Functionalization by the presence of second phase particles in the polymer matrix could improve the overall mechanical, thermal and electrical performance of the resulting composite. Examples of second phases include capsules for self-healing behavior (Kessler et al., 2003; Cohades et al., 2018), hollow microspheres to reduce the composite density (Porfiri and Gupta, 2009; Zhang et al., 2016) and powders to tailor capillary effects in porous structures (Kostornov et al., 2015). The introduction of these particles can however introduce complications in LCM processing. Filtration effects are commonly observed upon the infiltration of nanoparticles (Reia Da Costa et al., 2012; Yum et al., 2016; Zhang et al., 2017), which can even occur at fiber volume fractions of ~40% (Louis et al., 2014). A study by Louis et al. (Louis et al., 2019) showed that the filtration behavior of nanoparticles mainly depends on the particle size and the fiber volume fractions, while the nature, i.e., type of particle is also reported to have a large influence. The role of second phases on the capillary effects taking place in LCM processing is little understood. In their work on the processing of self-healing capsules, Manfredi and Michaud (Manfredi and Michaud, 2014) observed bilinear infusion rates, where, after an initial phase, the unsaturated permeability of the preforms strongly increased compared to that when no capsules were present. This was attributed to increased capillary effects that drive the flow in the presence of capsules, but no correlation between the particle concentration and the in-plane permeability was found. Caglar et al. (Caglar et al., 2017) tried to gain an improved understanding of these effects by a combination of in-plane permeability experiments and computational simulations. They confirmed that permeabilities increased in the presence of spherical glass; this was moreover found to depend on the bead diameter and the concentration in the composite. In a parallel study (Caglar et al., 2016), they reported on the influence of particle size and volume fraction on the capillary effects. They concluded that relatively small particles (40–70 μm and 100–200 μm) at low volume fractions enhanced the capillary effects, whereas an increase in the volume fraction resulted in a more homogenous pore distribution which yielded more balanced flows. On the other hand, large particles (400–800 μm) caused extensive deformation of the fabric layers and formation of new large flow channels resulted in less pronounced capillary flow enhancement.

Hierarchical composites have shown promising enhancements in mechanical, thermal and electrical performance (Thostenson et al., 2002; Yamamoto et al., 2009; Qian et al., 2010b; Chou et al., 2010; Spitalsky et al., 2010) when nanometer-spaced CNTs are grafted onto the fiber surfaces. With capillary pressure being inversely proportional to the channel diameter, strong capillary action (Futaba et al., 2006; Liu et al., 2006; Garcia et al., 2007) is induced in the presence of these

nanoporous CNT forests. Garcia et al. (Garcia et al., 2008) observed complete impregnation of their 80 nm-spaced CNT forests grafted on an alumina textile and suggested capillary effects to have contributed to this. Recent investigations by Staal et al. (Staal et al., 2021) on the permeability of the same fabric supported this suggestion. Induced capillary action by the presence of grafted CNTs can further be observed by fast droplet spreading over the surface of a single fiber (Qian et al., 2010a). Alternatively, Lee et al. (Lee et al., 2020) exploited the strong capillary actions induced by nanoporous networks of aligned CNTs for void-removal in Out-of-Autoclave (OoA) prepreg processing. Introduction of a nanoporous network between plies was estimated to increase the pressure gradient at the resin/void interface, i.e., the driving force for void removal, by 57% resulting in a void free composite, while a layup without these networks had a large void content. Moreover, resulting mechanical properties of the OoA-produced composites were like those achieved after conventional autoclave processing.

3.5.3 Capillary Effects in Thermoplastic LCM Processing

Influence of capillary effects in reactive thermoplastics and melt thermoplastics is strongly linked to their viscosity: for the reactive thermoplastics-based monomer (Rijswijk et al., 2009; Han et al., 2020; Obande et al., 2021), it is typically in the same range as or even lower than the viscosity of thermosetting polymers used in LCM processes while melt thermoplastics have a few orders of magnitude higher viscosities (Rijswijk et al., 2009; Salvatori et al., 2019; Han et al., 2020; Obande et al., 2021). In reactive systems, the capillary phenomena and their effects are similar to those found in thermosetting systems, but with enhanced capillary action resulting from the low viscosity of the fluid phase. For instance, Zingraff et al. (Zingraff et al., 2005) experimentally studied the resin transfer molding of a woven fabric with the precursor of an anionically polymerized polyamide 12 and also found an optimum capillary number range (in the order of 10^{-3}) where the void content was minimal. Similarly, Murray et al. (Murray et al., 2020) studied the resin transfer molding of unidirectional stitched glass fabrics with the precursor of in-situ polymerized polyamide six and demonstrated the dominance of viscous flow within the bundles as well as the void formation within bundles due to lack of balance between capillary and viscous forces. Melt thermoplastic impregnation is gaining importance in recent years, however capillary effects so far have not been analyzed (Studer et al., 2019; Gomez et al., 2021) as their impregnation is dominated by viscous forces due to the high-pressure differential and/or high viscosity of thermoplastic resins. Research is however ongoing to better capture the role of molecular weight and temperature in the wetting characteristics of polymers (Duchemin et al., 2021).

3.5.4 Capillary Effects in Continuous Composite Manufacturing

Next to LCM processes where the flow lengths can reach up to meters, capillary effects manifest themselves also in continuous composite manufacturing. For instance, resin bath impregnation pultrusion (Strauß et al., 2019; Vedernikov et al., 2020) is a

common technique for manufacturing fiber reinforced profiles of varying cross-sectional complexity. Irfan et al. (Irfan et al., 2017, 2021) modified the resin bath where the rovings are impregnated before entering the mold where they are shaped into the final cross-sectional profile. They demonstrated that in their modified pultrusion process, capillary impregnation was dominant owing to pre-spreading the fibers before entering the resin bath and the extended fluid reservoir promoting the capillary actions under low pressures. Another continuous composite route is the manufacturing of fiber reinforced (typically unidirectional) thermoplastic tapes that are then used in secondary processes such as automated fiber placement, press forming or in autoclave processes. Melt impregnation is generally used for thermoplastic tape manufacturing, as well as powder impregnation. In all cases, as well as in commingled yarns where reinforcement fibers and polymer fibers are intimately mixed, impregnation takes place after the polymer has melt, and capillary effects may again play a role towards local impregnation of the fiber tows. This was for example exploited by Ho et al. (Ho et al., 2011) for improving the quality of their wet powder impregnation approach, and by Bernet et al. (Bernet et al., 1999, 2001) for PA12/Carbon commingled yarns.

4 NUMERICAL MODELLING

Capillary effects play, despite the low magnitude of capillary pressures as compared to applied pressures, a significant role in LCM processing and, while mainly acting on a yarn-scale, largely influence the final part quality on a macroscopic scale. Capillary effects must thus be considered for the development of accurate numerical models that are used to describe and predict flow behavior in LCM. Several approaches have been proposed towards the development of flow simulations over the past decades, describing dual-scale flow behavior and the role of capillary effects at different scales. Most approaches base their estimation of the effects on direct or indirect experimental observation of flow front position, and saturation over time during an infiltration experiment, under no (apart from gravity) or applied external body forces.

4.1 Microscopic Scale Models
At the microscopic scale and under static conditions, the capillary pressure ΔP_γ is described as the pressure jump across the air-fluid interfaces arising from the solid surface and interfacial tensions defined by the Young–Laplace equation as previously described in **Section 2**. In the case of fibrous reinforcements, Ahn et al. (Ahn et al., 1991) and Pillai and Advani (Pillai and Advani, 1996) proposed an analytical expression of the capillary pressure, which was often used in later studies (Amico and Lekakou, 2000, Amico and Lekakou, 2001, Amico and Lekakou, 2002; Matsuzaki et al., 2015; Vilà et al., 2015; Willenbacher et al., 2019; Facciotto et al., 2021). They considered a tow, formed of several fibers with different spacing in size and thus with different capillary diameters impregnated with a unidirectional flow, and defined the capillary pressure as:

$$\Delta P_\gamma = \frac{V_f}{(1 - V_f)} \frac{F \sigma_{lv} \cos\theta}{D_f} \tag{4}$$

where F is a dimensionless shape factor describing the anisotropy of the tow (in general, F is assumed to be equal to 4 and 2 for longitudinal and transversal flows, respectively) and D_f is the fiber diameter. The term $\frac{V_f}{1-V_f}$ is known as the non-dimensional capillary pressure and represents the effect of the tow microstructure on the capillary pressure within the tow. Similarly, Bayramli and Powell (Bayramli and Powell, 1990) described the capillary pressure as:

$$\Delta P_\gamma = \frac{\sigma_{lv} \cos(\theta + \alpha)}{D_f (1 - \cos\alpha) + d} \tag{5}$$

where α is the directional body angle and d half of the minimum distance between two fibers. This model was improved by Foley and Gillespie (Foley and Gillespie, 2005) and later by Neacsu et al. (Neacsu et al., 2006). This equation has been used by Yeager et al. (Yeager et al., 2016; Yeager et al., 2017) and recently by Li et al. (Li et al., 2020) to describe the capillary pressure in their finite element models to simulate the resin moving in-between two fibers and thus model the injection of resin in a dual scale fabric in which the tows are quasi-realistically defined following a realistic model. Counterintuitively, the capillary pressure, which should not depend on the direction of flow, has been experimentally shown and modelled as indicated before as a function of flow direction with respect to the fiber preform. However, this is probably linked to the geometry of the pores and necks as the flow front progresses, indicating the influence of the pore-level scale onto the measurements.

In fluid infiltration, the capillary pressure is used for studying the local wettability between fiber and liquids, quantified by the contact angle θ. As infiltration involves motion, the dynamic contact angle is more accurate to describe the wettability between fluid and fibers. However, due to the complexity of determining it analytically, the static contact angle is usually measured for a first approximation even though it can strongly deviate from dynamic values. To overcome this, empirical laws such as Tanner's law (Tanner, 1979) are proposed in literature to estimate the dynamic contact angle from the static one. The static contact angle can be directly measured from e.g. from sessile drop or droplet-on-fiber measurements (Wu and Dzenis, 2006; Behroozi and Behroozi, 2019). In the case of structural fibers, a tensiometric method coupled to Wilhelmy's equation is usually applied to measure the dynamic contact angle and capillary forces (Pucci et al., 2016; Pucci et al., 2017a; Wang et al., 2017a; Hansen et al., 2017; Pucci et al., 2020). This method measures the force needed to pull or push a fiber or a tow partially submerged in a liquid as a function of the length of the immersed region. It is also possible to evaluate the of the meniscus profile between the fibers and the liquid. Similarly, some researchers performed wicking experiments on single tows (Hamdaoui et al., 2007; Pucci et al., 2015a; Koubaa et al., 2016; Castro et al., 2020) or a single layer of fabric (Lebel et al., 2013; Pucci et al., 2015b, Pucci et al., 2016; Vo et al., 2020) and were able to extract the values of the capillary pressure and the dynamic advancing contact angle using the Lucas-Washburn
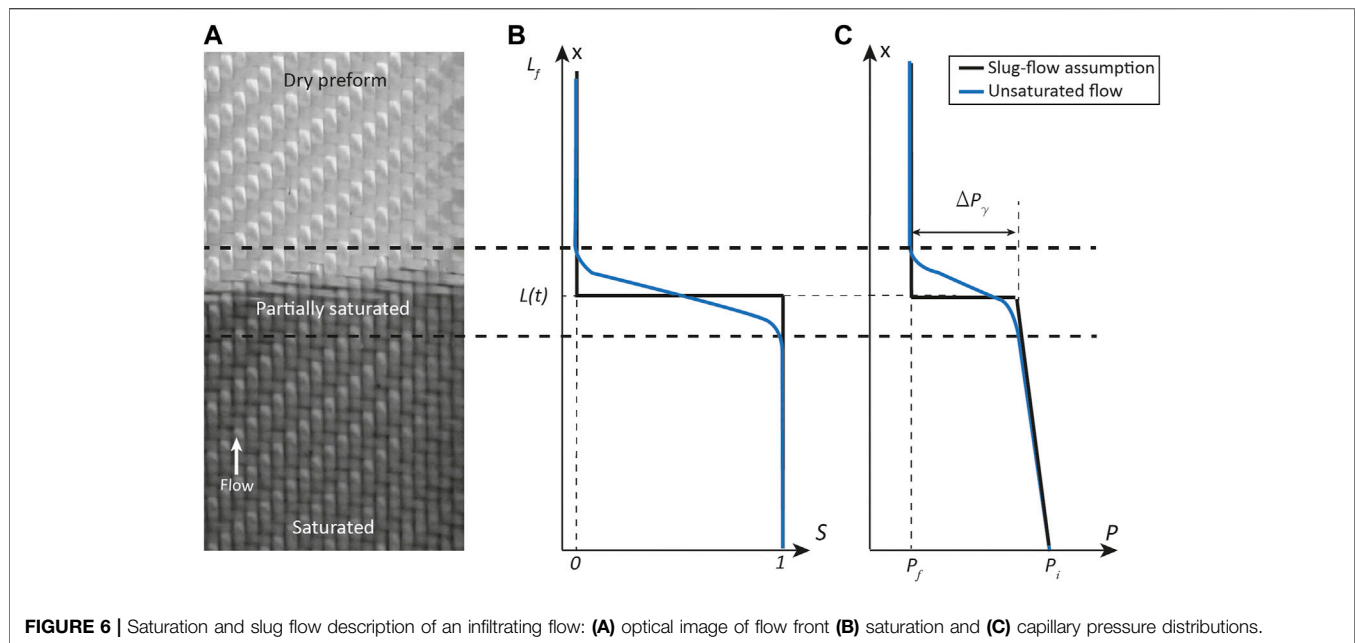
FIGURE 6 | Saturation and slug flow description of an infiltrating flow: **(A)** optical image of flow front **(B)** saturation and **(C)** capillary pressure distributions.

method (Washburn, 1921) which describes the capillary rise of a liquid inside a capillary tube, and by extension into a porous media. However, the Lucas-Washburn approach assumes a constant geometry of the porous medium during the experiment and does not take into account attraction forces between vertical cylinders resulting from elasto-capillary effects and neither the swelling effect in natural fibers which leads to densification phenomenon, this is why some modifications have been proposed over the years (Rieser et al., 2015; Koubaa et al., 2016; Pucci et al., 2016; Vo et al., 2020). Lebel et al. (LeBel et al., 2014) proposed a simple methodology to obtain the optimal flow injection conditions for a given fluid/fabric system based on the Lucas-Washburn imbibition model, which was thereafter used in Refs. (Ravey et al., 2014; Causse et al., 2018; LeBel et al., 2019; Castro et al., 2021).

4.2 Unsaturated Flow Models

Capillary effects are also included in studies at the more macroscopic scale and are regarded as promoters of micro-diffusion inside the tows. Since the dual scale of the fabrics leads to a multiphase flow effect, it is commonly accepted that the fibrous preform is progressively saturated by the liquid, resulting in a nonlinear pressure profile along the unsaturated area (**Figure 6**). Partially saturated regions indeed show a broad distribution of pore channel diameters and thereby capillary forces act at a wide range of scales, therefore in macroscopic studies, the capillary pressure is represented by an average of multiple capillary pressure jumps inside a small region (RVE). Moreover, the progressive saturation is directly linked to a progressive filling of the pores and can be in turn related to void mechanisms during the infiltration (Park and Lee, 2011; LeBel et al., 2017). Two main strategies are commonly adopted to tackle unsaturated flow phenomena: two-phase flow and dual-scale approaches (Michaud, 2016).

The first approach is inspired from soil science and relies on traditional multiphase flow equations for porous media (Panfilov, 2000). Although this approach is commonly used in other branches of engineering, researchers seldom applied it to model composite infiltration processes (Bréard et al., 2003a; Nordlund and Michaud, 2012; Gascón et al., 2015; Villière et al., 2015; Gascón et al., 2016). Resin flow is in this case modelled as a two-phase flow in which the resin invades the porous medium (fabric), displacing and expelling the fluid which saturates the porous medium (air). As already discussed, depending on the fiber/matrix system and the impregnation conditions (fluid velocity), resin and air can be either wetting (*w*) and non-wetting (*nw*). For simplicity, the resin is often considered to be the non-wetting phase, which is often observed to be the case in industrial LCM processing when flow is fast enough that the dynamic contact angle becomes greater than 90°. In the current method, permeability and pressure are dependent on the infiltrating fluid saturation *S* and the sum of the phase's saturations are equal to 1. If the porous medium is assimilated to a random assembly of tubes of various radii, each of these tubes will drain the fluid differently and a strong relationship is created between the saturation and the capillary pressure, defined as the pressure difference between the two phases as:

$$\Delta P_\gamma (S) = P_{nw} - P_w \tag{6}$$

There are two main approaches to tackle the modeling. One is the two-pressure formulation which uses mass balance equations and a single-phase Darcy's law to describe the velocity of the two fluids through the same porous material. If the air pressure is assumed to be relatively low, the mass balance equation for the resin can be solved independently and is reduced to Richard's equation (Nordlund and Michaud, 2012). The other approach is the fractional flow method, which considers saturation and

pressure as independent variables. Gravitational and capillary pressures are neglected and saturation is defined by the Buckley-Leverett formulation (which assumes an isotropic medium) (Buckley and Leverett, 1942). Gascón et al. (Gascón et al., 2015; Gascón et al., 2016) more recently proposed a numerical model based on this approach which includes capillary effects and the effect of air residual saturation. In two phase flow modeling, the permeability K is divided into two terms $K = k_r K_{sat}$, where K_{sat} is the saturated permeability and k_r the relative permeability, a dimensionless value between 0 and 1 which is a function of S. The relative permeability is defined for both phases as $k_{r,nw}$ and $k_{r,w}$, and describes how fluid and air phases flow with respect to each other into the porous medium. Two phase flow formulations require constitutive equations between the permeability, the resin saturation and the capillary pressure. Different analytical parameterizations have been proposed to define $k_r(S)$ and $S(P)$, usually defined by a power law such as the functional descriptions of Brooks and Corey (Brooks and Corey, 1964) and Van Genuchten (van Genuchten, 1980), among others (Hassanizadeh and Gray, 1990; Helmig et al., 2007; Gao et al., 2014). These formulations can also be obtained with the help of parametric studies of virtual fibrous microstructures, as proposed by Ashari and Vahedi Tafreshi for thin fibrous sheets (Ashari and Vahedi Tafreshi, 2009). Bréard et al. (Bréard et al., 2003a) introduced a relative permeability law specifically for fibrous reinforcements based on the ratio of unsaturated and saturated permeability R_s which will be introduced thereafter. $S(P)$ curve is known in soil science as the imbibition-drainage curve. Drainage is used to indicate when a non-wetting fluid displaces a wetting fluid whereas imbibition indicates when a wetting fluid displaces a non-wetting fluid. Nordlund et al. (Nordlund and Michaud, 2012) used the semi-empirical expression developed by van Genuchten and Mualem (Mualem, 1978; van Genuchten, 1980) to model the impregnation of a glass preform by a resin; they observed a strong dependence between the saturation curve and flow rate given the dynamic wetting conditions during the impregnation. As a result, they showed that several imbibition-drainage curves may be necessary to model flow over a wider range of velocities. Similarly, Gascón et al. (Gascón et al., 2015; Gascón et al., 2016) used a formulation based on that of Brooks and Corey to model the saturation in a glass fiber reinforcement to predict void formation and transport mechanisms. With this approach, it is not possible to a priori determine the location of voids as a similar degree of saturation could correspond to voids in the tows or in between, nonetheless the dependency of the saturation curve on flow rate may be an indirect indication of a change in void location.

The second approach is more specific to the polymer composite processing field and considers the preform as a dual-scale body, separating the intra- and inter-bundle impregnations by introducing a sink term into fully saturated models (Bréard et al., 2003a; Simacek and Advani, 2003; Gourichon et al., 2006; Wolfrath et al., 2006; Bayldon and Daniel, 2009; Lawrence et al., 2009; Wang et al., 2009; Simacek et al., 2010; Park and Lee, 2011; Tan and Pillai, 2012; Walther et al., 2012; Carlone and Palazzo, 2015; Carlone et al., 2018; Imbert et al., 2018; Patiño-Arcila and Vanegas-Jaramillo,

2018; Wu and Larsson, 2020; Facciotto et al., 2021; Patiño and Nieto-Londoño, 2021). These models consider that viscous forces dominate (non-wetting system) the infiltration and that the flow preferentially fills the inter-tow macro. The bundles upstream are gradually saturated by a delayed secondary micro flow altering the overall pressure as shown in **Figure 7**. The capillary pressure will in this case influence only the time to saturate the tows.

Generally, the length of the partially saturated zone is assumed to be constant. Then, the pressure drop creates an apparent change in the permeability and this delayed effect is considered by adding a sink term $\dot{S}$ into the common equations which represent the liquid saturation or volume rate into the fiber tow. In this approach, tow and overall fabric permeability are usually measured in saturated models. However, for higher accuracy, some researchers proposed to model the permeability in terms of degree of saturation or void content (Lawrence et al., 2009; Simacek et al., 2010). The mass conservation equation can then be written as:

$$\dot{S} = \nabla\left(\frac{K}{\eta_{resin}}\nabla P\right) \qquad (7)$$

If the flow front is non-uniform (i.e., intra- or inter-yarn flow is predominant), $\dot{S}$ is not null and the relationship between pressure and time is not linear anymore which in turn influences the overall permeability (Bodaghi et al., 2019). Longitudinal dual-scale flow analysis is usually performed by using a Stokes-Darcy or a Stokes-Brinkman coupling (with the latter one being more common) (Patiño et al., 2017; Lu et al., 2021). The Stokes equation is employed to define the inter-tow flow and the Darcy or Brinkman equations for the intra-tow flow. A coupling condition is developed at the interface to ensure a mass transfer from the inter- to the intra-tow flow. This approach is usually linked to void entrapment and void migration models (Mehdikhani et al., 2019). Given the dual-scale nature of fabrics, some authors worked on the combined interaction between intra- and inter-tow permeability on the global permeability (Bodaghi et al., 2019). Bréard et al. (Bréard et al., 2003a) measured a convex pressure curve profile along the impregnation, explained by the delayed tow saturation. Park and Lee (Park and Lee, 2011) later assimilated a convex and/or concave shape to the pressure curve, depending on the presence of capillary effects as shown in **Figure 8**. If the degree of saturation is lower than 1, unsaturated permeability is lower but close to the saturated permeability, a convex profile is obtained. If the degree of saturation drops and is far from 1, capillary effects are more significant and tow saturation is more prominent.

The Control Volume Finite Element approach has been a preferred route for homogenized simulations to predict the flow evolution, fill times, and has been used for process optimization of RTM and its variants such as VARTM (Correia et al., 2004; Sas et al., 2015; Wang et al., 2016, 2017b; Caglar et al., 2021b; Chai et al., 2021) as well as for purposes such as predicting the formation of macroscale voids (Park et al., 2011; Park and Lee, 2011), predicting the permeability (Lugo et al., 2014; Yun et al., 2017; Caglar et al., 2018; Godbole et al., 2019) and changes in the flow patterns induced by inserts or race-tracking channels
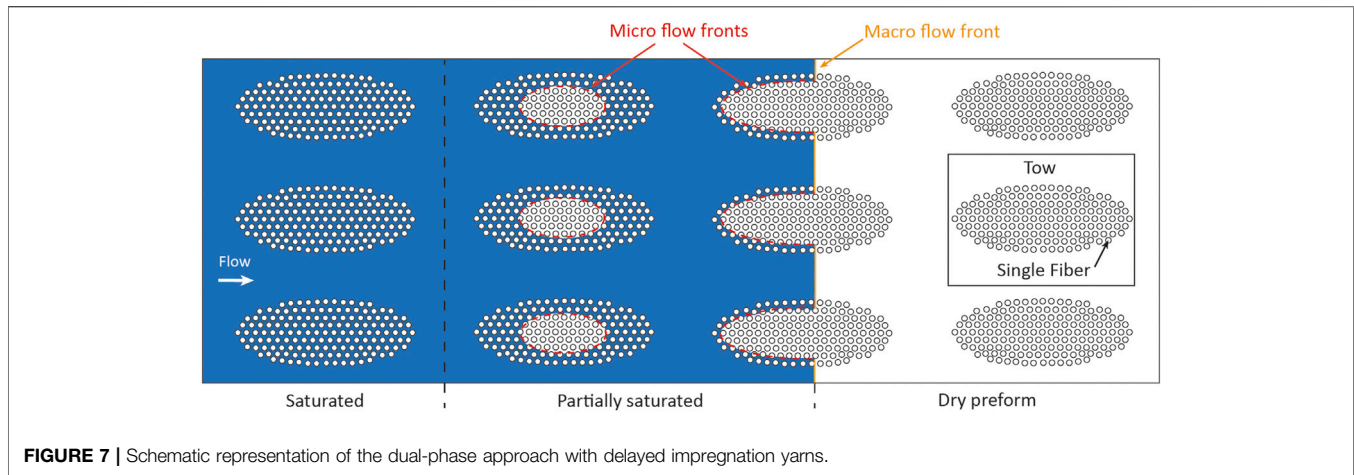
FIGURE 7 | Schematic representation of the dual-phase approach with delayed impregnation yarns.
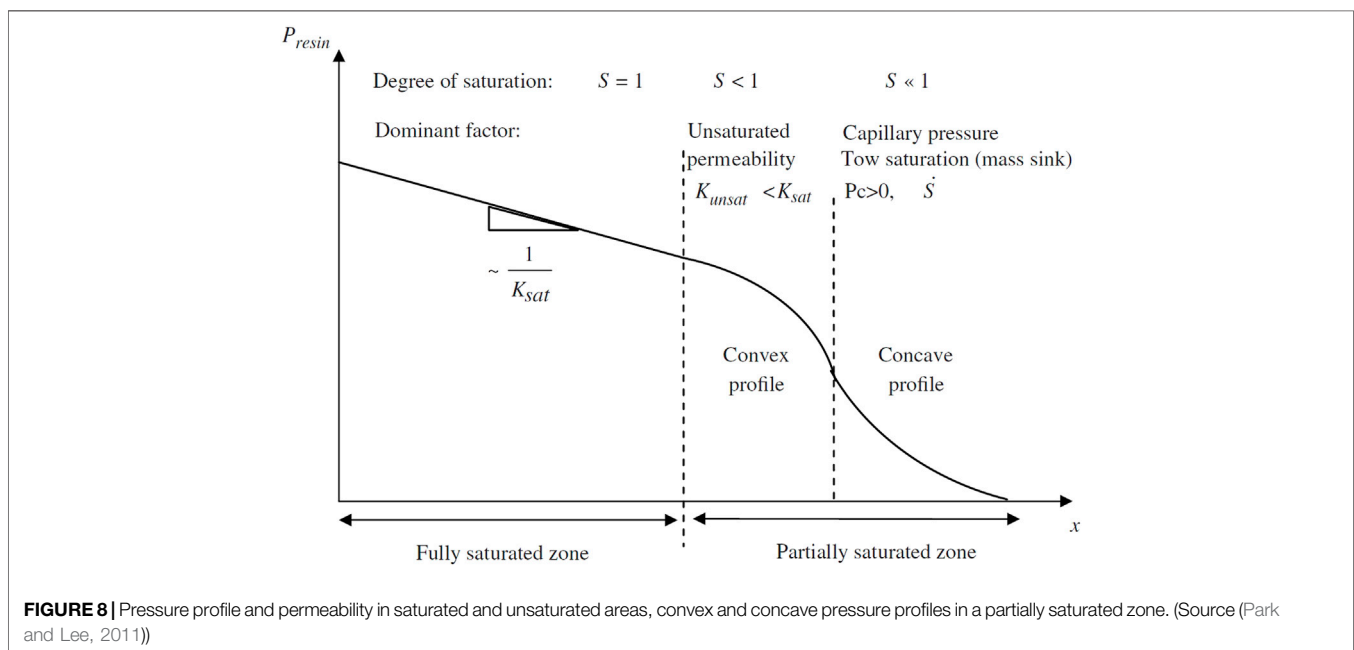

FIGURE 8 | Pressure profile and permeability in saturated and unsaturated areas, convex and concave pressure profiles in a partially saturated zone. (Source (Park and Lee, 2011))

as well as in part manufacturing around inserts (Matsuzaki et al., 2013; Sas et al., 2015; Pierce and Falzon, 2017) and as a predictive tool in active control of these processes (Alms et al., 2011; Matsuzaki et al., 2013). Several works have made use of existing flow simulation software such as LIMS and introduced additional terms to account for the dual scale effects (Schell et al., 2007; Lawrence et al., 2009; Simacek et al., 2010; Facciotto et al., 2021). Similarly, finite element solvers are coupled with level-set for tracking the free surface and enriched for accounting for multiscale effects at the air-liquid-solid interface (Liu et al., 2016; Chevalier et al., 2018; Andriamananjara et al., 2019; Rougier et al., 2021) with capability of modeling wetting and non-wetting systems as well as the transition or to predict the average capillary pressure evolution in between individual fibers (Yeager et al., 2016). In recent years, there has also been interest towards the use

of other numerical approaches to account for the dual scale effects using particle based solvers (Yashiro et al., 2019; Yoshihara et al., 2020) or boundary elements (Patiño and Nieto-Londoño, 2021). Recent developments in application of above mentioned in modeling the dual-scale flow with a focus on the introduction of sink effects has been reviewed by Patiño-Arcila and Vanegas-Jaramillo (Patiño-Arcila and Vanegas-Jaramillo, 2018).

4.3 Slug-Flow Assumption

For simplicity, it is often considered that the liquid progresses with a fully saturated front neglecting preferential flow channeling, known as the "slug-flow" assumption. As shown in **Figure 6**, the saturation results in a step function varying between 0 and 1 (the steady-state saturation can be less than one if voids remain entrapped behind the flow front). Although capillary effects arise from local micro-scale geometric and

surface tension mechanisms, they are in this case considered as a macro phenomenon and are lumped in the conventional fluid flow equations as a pressure difference ΔP_γ. This pressure created at the flow front compensates the delayed flow coming from the low permeability of the packed tows (Amico and Lekakou, 2001). The total fluid pressure difference ΔP can be defined as the applied pressure difference ΔP_{app} between the inlet (i) and the outlet (f) considering the capillary forces:

$$\Delta P = P_f - P_i + \Delta P_\gamma = \Delta P_{app} + \Delta P_\gamma \qquad (8)$$

The capillary pressure can be expressed as:

$$\Delta P_\gamma = -S_f \sigma_{lv} \cos \theta \qquad (9)$$

where S_f is the total surface of matrix-fiber interfaces per unit of volume (Mortensen and Cornie, 1987; Mortensen and Wong, 1990). The capillary pressure drop ΔP_γ can be quantified within an experiment in which the fluid is injected into the preform either at constant pressure or constant flow rate. In unidirectional cases it is possible to track the fluid movement using Darcy's law and the Dupuit-Forchheimer approximation and find the ΔP_γ value from experimental results (Amico and Lekakou, 2001; Zingraff et al., 2005; Verrey et al., 2006; Li et al., 2010; Li et al., 2012). Verrey et al. (Verrey et al., 2006) proved that it is more suitable to measure ΔP_γ in a constant flow rate experiment rather than constant pressure experiment, since in the latter, the velocity changes significantly during impregnation resulting in a decreasing range of capillary numbers.

Intuitively, capillary effects taking place at the flow front can alter the fluid velocity leading to erroneous unsaturated permeability measurements. Although unsaturated (K_{unsat}) and saturated (K_{sat}) permeabilities are respectively measured from the flow front position and the flow rate after filling the textile, they should be theoretically equal as they only depend on the fabric structure. Nevertheless, significant differences between these two values have been reported in literature (Lundström et al., 2000; Bréard et al., 2003a; Pillai, 2004; Kim et al., 2017). Whereas some authors support that the saturated permeability should be higher than the unsaturated permeability because dry tows oppose a certain resistance to the macro-flow, the opposite has also been observed. By using a slug flow approach, one can show that the capillary pressure drop acting at the flow front should be taken into account when estimating the unsaturated permeability, whereas it is generally omitted. As a result, the permeability ratio R_s is also easily expressed as a function of the ratio of capillary over applied pressure (Salvatori et al., 2018):

$$R_s = \frac{K_{unsat}}{K_{sat}} = 1 - \frac{\Delta P_\gamma}{\Delta P_{app}} \qquad (10)$$
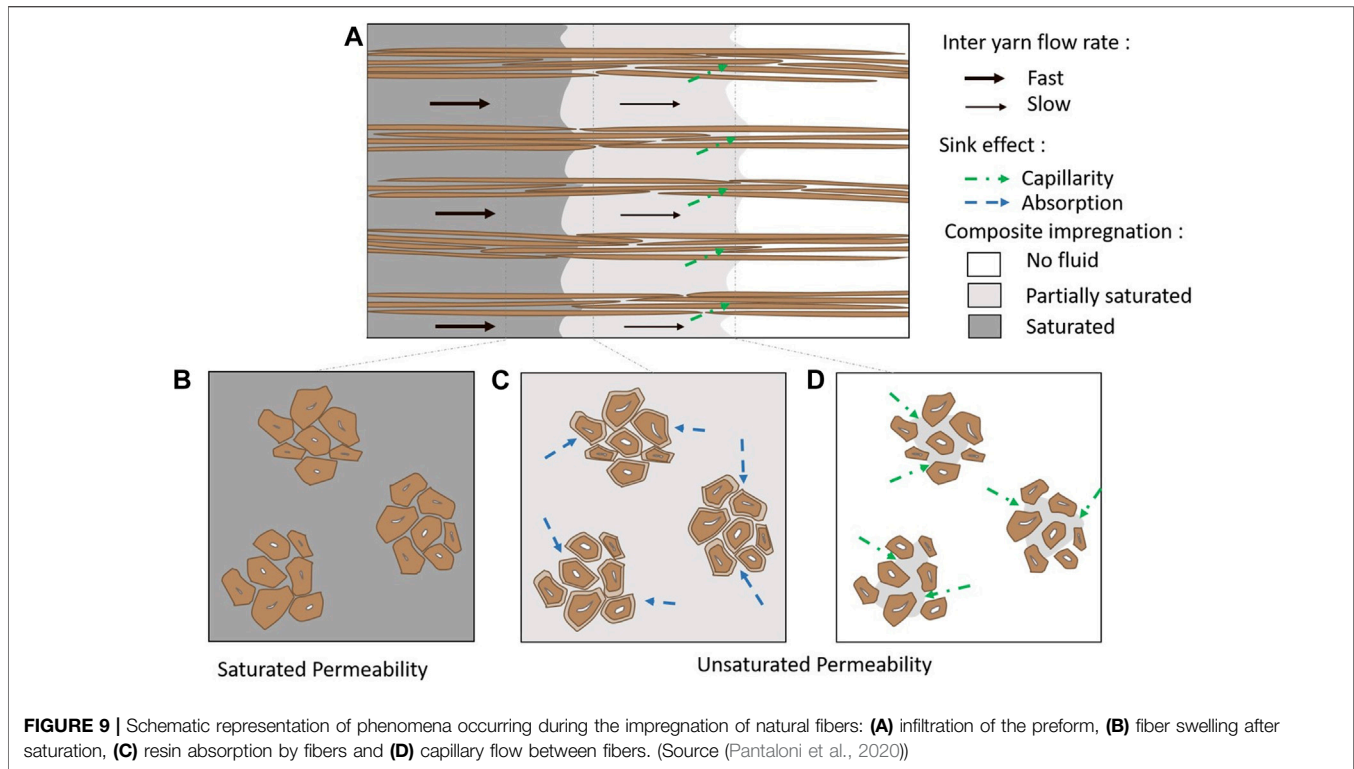
Since ΔP_γ is directly dependent on the capillary number and thus the dynamic wettability of the system, K_{unsat} turns to be not only fabric architecture dependent, but also relies on the fluid-fabric wettability. Following this approach, if infiltration is carried out under conditions close to the optimal capillary number, capillary effects may be negligible and R_s will be equal to 1. On the contrary, if ΔP_γ is not negligible, the two permeability values will differ. If ΔP_γ is negative, at least when estimated locally

close to the tows, the system is wetting and $R_s > 1$ and conversely, if ΔP_γ is positive, the system is non-wetting and $R_s < 1$. The ratio R_s was observed to be generally below 1, considering that the fluid acts with a non-wetting behavior (Bréard et al., 2003a) even though values above 1 have also been observed in the case of slow flow (Lundström et al., 2000). However, it is important to note that the geometric features of the porous medium also have an effect, and optimal Ca flow conditions have been found in cases where ΔP_γ is negative, at least when estimated close to the tows, such that the capillary forces inside the tows compensate for their lower permeability to reach a stable front. This was observed by Gueroult et al. (Gueroult et al., 2014), who proposed an analytical model evaluating the time scales for flow in each of the two regions, tow and inter-tow channels.

Nowadays, the use of K_{unsat} as a measurement of the permeability is still debated since it is influenced by capillary effects. For example, several authors observed that the fiber volume fraction influences R_s due to the increase of tows and micro spaces leading to an increase of capillary phenomena and in turn a change of the unsaturated permeability (Francucci et al., 2010; Caglar et al., 2019; Moudood et al., 2019). The choice of model fluids to measure permeability also becomes highly critical since their surface tension and viscosity should be close enough to those of the resin. Overall, this measurement is fine for comparative purposes if the same fluids and conditions are used, as was demonstrated in the round robin exercise (Vernet et al., 2014).

Salvatori et al. (Salvatori et al., 2018) studied the effect of the fabric architecture on permeability and capillary effects. They showed for a classic woven fabric, that R_s is greater than 1 at low capillary numbers, below 1 for high capillary numbers and around 1 close to the optimal infiltration conditions. For a fabric with large meso-channels, R_s was found to be close to 1 for a wide range of capillary numbers since inter-tow flow dominates the overall flow kinetics and capillary effects are insignificant. They concluded that unsaturated permeability can be used as a permeability measurement for fabrics showing a strong-dual scale nature. Caglar et al. (Caglar et al., 2019) improved the wetting characteristics of a glass fabric by means of corona treatment without altering the permeability. They found similar permeability values for pristine and treated fabrics, however, they proved that the change in the wettability has a strong effect on the R_s. Impregnation of treated fabrics is enhanced by the wettability of the system translated to an increase of K_{unsat} with R_s is higher than 1. Conversely, for the pristine fabrics the system remains non-wetting and R_s is lower than 1. Recently, Staal et al. (Staal et al., 2021) studied the permeability of alumina fiber woven fabrics grafted with aligned carbon nanotubes (CNT). They found R_s values to be higher than 1 in all cases attributed to the capillary wicking happening in the forest areas created by the CNT. In this case, the flow is dragged by capillary forces leading to a strong wetting system. This observation is also consistent with models of wetting on rough surfaces, indicating that wettability can be enhanced when the surface roughness is increased.

In the case of natural fibers, it is usually observed that K_{unsat} is lower than K_{sat}. As already introduced, infiltration is hampered by the fibers absorption behavior which removes fluid from the

FIGURE 9 | Schematic representation of phenomena occurring during the impregnation of natural fibers: **(A)** infiltration of the preform, **(B)** fiber swelling after saturation, **(C)** resin absorption by fibers and **(D)** capillary flow between fibers. (Source (Pantaloni et al., 2020))

main stream (**Figure 9**), reducing the macro flow velocity and in consequence, directly affecting the unsaturated permeability. Since the sink effect is highly influenced by the nature of the infiltrating fluid, permeability measurements will be highly fluid type dependent (Nguyen et al., 2014; Moudood et al., 2019). Thereupon, fibers will continue to absorb liquid until their saturation leading to fiber swelling and thus changing the fibrous microstructure. Consequently, the fiber volume fraction is increased, reducing the fluid path and directly influencing the saturated permeability. Nguyen et al. (Nguyen et al., 2014) showed that the fiber diameter after swelling is also influenced by liquid nature, in turn, the saturated permeability is also fluid type dependent. Thus, both unsaturated and saturated permeability are reduced due to absorption and swelling respectively, however, it has always been observed that $K_{unsat} > K_{sat}$ absorption thus being more critical than swelling. Nevertheless, researchers showed that at low fiber volume fraction, this behavior is reversed ($K_{unsat} < K_{sat}$) since less amount of fibers are present, less fluid is removed from the stream and the change in the macro flow is insignificant (Francucci et al., 2010; Moudood et al., 2019; Pantaloni et al., 2020).

5 CONCLUSION

Capillary effects operate at several length scales in composite processing, from the molecular scale at the triple line between fluid, solid and air, which can be related to the physical characteristics of the phases, to the scale of the spaces within fiber tows or between tows, which are related to the geometrical features of the reinforcement. They are generally not the main drivers of flow in composite processing, where external pressure or flow rates are imposed on the fluid phase to speed the flow kinetics. However, they have been shown to play a crucial role in determining the part quality; the consensus is now large in our community that there is an optimal flow front velocity to minimize porosity entrapment during impregnation of a fiber reinforcement textile, which corresponds to an optimal capillary number Ca_{opt} ranging between 0.5 and $1.5 \cdot 10^{-3}$ depending on the fabric type and to a minor extent, conditions of experiments. There is also an increasing consensus on the utility to measure unsaturated and saturated permeabilities and to evaluate their ratio to better quantify macro-scale capillary effects, although often using model fluids. Research is very active these days to improve our experimental understanding of these effects thanks to the increasing availability of time- and space-resolved experimental observation tools, and computing power as well as a technological pull to further improve part quality and production robustness. However, modelling is still in progress to link local wetting effects with geometrical pore effects leading to macroscopic volume averaged capillary effects, as also observed in the soil science field, although microscopic and macroscopic effects tend to be independently increasingly well captured.

It is clear to all composite manufacturers that relying only on capillary effects to impregnate a composite is not practical, even if the static contact angle seems very low and the system is wetting, as the flow kinetics would be too low (depending on the fluid viscosity) and the quality poor, due to porosity forming in between the wicking tows. In some cases, when the porous

medium is more uniform or when a very fine porous network is placed between fibers, as in CNT grafted fabrics, enhanced capillary effects may help drive the flow and counteract a reduced overall permeability. This effect could also be taken advantage of when flow takes place at short distance, for example in thermoplastic composite processing from stacked films, fibers or powders.

In most practical cases however, the need to reduce cycle times led to the development of more permeable textiles, with increased dual scale pore space distribution (wider flow channels and more compact tows), and flow takes place well above the optimal capillary number. This often leads to a delay in tow impregnation, with potential porosity remaining within the tows, or the practice to let resin flow out for some time to saturate the fabric. This could possibly be minimized with enhanced local wetting at the tow level if air can find a path to escape ahead of the flow front. As a result, well distributed and optimized sizings could still play a strong role not only for mechanical properties, but also to ensure optimal flow conditions.

AUTHOR CONTRIBUTIONS

All authors listed have made a substantial, direct, and intellectual contribution to the work and approved it for publication.

ACKNOWLEDGMENTS

REFERENCES

Abdelwahed, M. A. B., Wielhorski, Y., Bizet, L., and Bréard, J. (2014). Bubble Formation and Transport in T-junction for Application to Liquid Composite Molding: Wetting Effect. *J. Compos. Mater.* 48, 37–48. doi:10.1177/0021998312467553

Ahn, K. J., Seferis, J. C., and Berg, J. C. (1991). Simultaneous Measurements of Permeability and Capillary Pressure of Thermosetting Matrices in Woven Fabric Reinforcements. *Polym. Compos.* 12, 146–152. doi:10.1002/pc.750120303

Ali, M. A., Umer, R., Khan, K. A., and Cantwell, W. J. (2019). In-plane Virtual Permeability Characterization of 3D Woven Fabrics Using a Hybrid Experimental and Numerical Approach. *Composites Sci. Techn.* 173, 99–109. doi:10.1016/j.compscitech.2019.01.030

Alms, J. B., Advani, S. G., and Glancey, J. L. (2011). Liquid Composite Molding Control Methodologies Using Vacuum Induced Preform Relaxation. *Composites A: Appl. Sci. Manufacturing* 42, 57–65. doi:10.1016/j.compositesa.2010.10.002

Amico, S. C., and Lekakou, C. (2002). Axial Impregnation of a Fiber Bundle. Part 2: Theoretical Analysis. *Polym. Compos.* 23, 264–273. doi:10.1002/pc.10430

Amico, S., and Lekakou, C. (2001). An Experimental Study of the Permeability and Capillary Pressure in Resin-Transfer Moulding. *Composites Sci. Techn.* 61, 1945–1959. doi:10.1016/S0266-3538(01)00104-X

Amico, S., and Lekakou, C. (2000). Mathematical Modelling of Capillary Micro-flow through Woven Fabrics. *Composites Part A: Appl. Sci. Manufacturing* 31, 1331–1344. doi:10.1016/S1359-835X(00)00033-6

Andriamananjara, K., Moulin, N., Bruchon, J., Liotier, P.-J., and Drapier, S. (2019). Numerical Modeling of Local Capillary Effects in Porous media as a Pressure Discontinuity Acting on the Interface of a Transient Bi-fluid Flow. *Int. J. Mater. Form.* 12, 675–691. doi:10.1007/s12289-018-1442-3

Araujo, Y. C., Toledo, P. G., Leon, V., and Gonzalez, H. Y. (1995). Wettability of Silane-Treated Glass Slides as Determined from X-Ray Photoelectron Spectroscopy. *J. Colloid Interf. Sci.* 176, 485–490. doi:10.1006/jcis.1995.9942

Armstrong, R. T., Sun, C., Mostaghimi, P., Berg, S., Rücker, M., Luckham, P., et al. (2021). Multiscale Characterization of Wettability in Porous Media. *Transp Porous Med.* 140, 215–240. doi:10.1007/s11242-021-01615-0

Ashari, A., and Vahedi Tafreshi, H. (2009). General Capillary Pressure and Relative Permeability Expressions for Through-Plane Fluid Transport in Thin Fibrous Sheets. *Colloids Surf. A: Physicochemical Eng. Aspects* 346, 114–122. doi:10.1016/j.colsurfa.2009.06.001

Bayldon, J. M., and Daniel, I. M. (2009). Flow Modeling of the VARTM Process Including Progressive Saturation Effects. *Composites Part A: Appl. Sci. Manufacturing* 40, 1044–1052. doi:10.1016/j.compositesa.2009.04.008

Bayramli, E., and Powell, R. L. (1990). The normal (Transverse) Impregnation of Liquids into Axially Oriented Fiber Bundles. *J. Colloid Interf. Sci.* 138, 346–353. doi:10.1016/0021-9797(90)90217-C

Bear, J. (1972). *Dynamics of Fluids in Porous Media*. New York, NY: American Elsevier Publishing Company.

Behroozi, F., and Behroozi, P. S. (2019). Reliable Determination of Contact Angle from the Height and Volume of Sessile Drops. *Am. J. Phys.* 87, 28–32. doi:10.1119/1.5078512

Bencsik, M., Adriaensen, H., Brewer, S. A., and McHale, G. (2008). Quantitative NMR Monitoring of Liquid Ingress into Repellent Heterogeneous Layered Fabrics. *J. Magn. Reson.* 193, 32–36. doi:10.1016/j.jmr.2008.04.003

Bernet, N., Bourban, P.-E., and Maånson, J.-A. E. (2000). On the Characterization of Wetting and Adhesion in Glass fiber-PA12 Composites. *J. Thermoplastic Compos. Mater.* 13, 434–450. doi:10.1106/W3B4-CFKP-02VR-OXTE

Bernet, N., Michaud, V., Bourban, P.-E., and Manson, J.-A. E. (1999). Impregnation Model for the Consolidation of Thermoplastic Composites Made from Commingled Yarns. *J. Compos. Mater.* 33. doi:10.1177/002199839903300806

Bernet, N., Michaud, V., Bourban, P. E., and Månson, J. A. E. (2001). Commingled Yarn Composites for Rapid Processing of Complex Shapes. *Compos. - Part A. Appl. Sci. Manuf.* 32. doi:10.1016/S1359-835X(00)00180-9

Bijeljic, B., D. Mantle, M., J. Sederman, A., F. Gladden, L., and D. Papathanasiou, T. (2004). Slow Flow across Macroscopically Semi-circular Fibre Lattices and a Free-Flow Region of Variable Width-Visualisation by Magnetic Resonance Imaging. *Chem. Eng. Sci.* 59, 2089–2103. doi:10.1016/j.ces.2004.02.007

Binetruy, C., Hilaire, B., and Pabiot, J. (1998). Tow Impregnation Model and Void Formation Mechanisms during RTM. *J. Compos. Mater.* 32, 223–245. doi:10.1177/002199839803200302

Bodaghi, M., Lomov, S. V., Simacek, P., Correia, N. C., and Advani, S. G. (2019). On the Variability of Permeability Induced by Reinforcement Distortions and Dual Scale Flow in Liquid Composite Moulding: A Review. *Composites Part A: Appl. Sci. Manufacturing* 120, 188–210. doi:10.1016/j.compositesa.2019.03.004

Bonnard, B., Causse, P., and Trochu, F. (2017). Experimental Characterization of the Pore Size Distribution in Fibrous Reinforcements of Composite Materials. *J. Compos. Mater.* 51, 3807–3818. doi:10.1177/0021998317694424

Bréard, J., Saouab, A., and Bouquet, G. (1999). Dependence of the Reinforcement Anisotropy on a Three Dimensional Resin Flow Observed by X-Ray Radioscopy. *J. Reinforced Plastics Composites* 18, 814–826. doi:10.1177/073168449901800903

Bréard, J., Henzel, Y., Trochu, F., and Gauvin, R. (2003a). Analysis of Dynamic Flows through Porous media. Part I: Comparison between Saturated and Unsaturated Flows in Fibrous Reinforcements. *Polym. Compos.* 24, 391–408. doi:10.1002/pc.10038

Bréard, J., Saouab, A., and Bouquet, G. (2003b). Numerical Simulation of Void Formation in LCM. *Composites Part A: Appl. Sci. Manufacturing* 34, 517–523. doi:10.1016/S1359-835X(03)00055-1

Brooks, R., and Corey, A. (1964). *Hydraulic Properties of Porous media*. Fort Collins: Colorado State University Hydrology. Papers Available at: http://www.citeulike.org/group/1336/article/711012.

Buckley, S. E., and Leverett, M. C. (1942). Mechanism of Fluid Displacement in Sands. *Trans. AIME* 146, 107–116. doi:10.2118/942107-g

Bull, D. J., Spearing, S. M., Sinclair, I., and Helfen, L. (2013). Three-dimensional Assessment of Low Velocity Impact Damage in Particle Toughened Composite Laminates Using Micro-focus X-ray Computed Tomography and Synchrotron Radiation Laminography. *Composites Part A: Appl. Sci. Manufacturing* 52, 62–69. doi:10.1016/j.compositesa.2013.05.003

Caglar, B., Esposito, W., Nguyen-Dang, T., Laperrousaz, S., Michaud, V., and Sorin, F. (2021a). Functionalized Fiber Reinforced Composites via Thermally Drawn Multifunctional Fiber Sensors. *Adv. Mater. Technol.* 6, 2000957–2000958. doi:10.1002/admt.202000957

Caglar, B., Hancioglu, M., and Sozer, E. M. (2021b). Monitoring and Modeling of Part Thickness Evolution in Vacuum Infusion Process. *J. Compos. Mater.* 55, 1053–1072. doi:10.1177/0021998320963173

Caglar, B., Michaud, V., and Sozer, E. M. (2016). "Experimental Investigation of Textile Permeability in the Presence of Spherical Inclusions," in ECCM 2016 - Proceeding 17th European Conference on Composite Materials, Munich, Germany, June 26–30, 2016, 26–30.

Caglar, B., Orgéas, L., Rolland du Roscoat, S., Sozer, E. M., and Michaud, V. (2017). Permeability of Textile Fabrics with Spherical Inclusions. *Composites Part A: Appl. Sci. Manufacturing* 99, 1–14. doi:10.1016/j.compositesa.2017.03.031

Caglar, B., Salvatori, D., Sozer, E. M., and Michaud, V. (2018). In-plane Permeability Distribution Mapping of Isotropic Mats Using Flow Front Detection. *Composites Part A: Appl. Sci. Manufacturing* 113, 275–286. doi:10.1016/j.compositesa.2018.07.036

Caglar, B., Tekin, C., Karasu, F., and Michaud, V. (2019). Assessment of Capillary Phenomena in Liquid Composite Molding. *Composites Part A: Appl. Sci. Manufacturing* 120, 73–83. doi:10.1016/j.compositesa.2019.02.018

Callaghan, P. T. (1993). *Principles of Nuclear Magnetic Resonance Microscopy.* Oxford: Oxford University Press.

Carlone, P., and Palazzo, G. S. (2015). Unsaturated and Saturated Flow Front Tracking in Liquid Composite Molding Processes Using Dielectric Sensors. *Appl. Compos. Mater.* 22, 543–557. doi:10.1007/s10443-014-9422-3

Carlone, P., Rubino, F., Paradiso, V., and Tucci, F. (2018). Multi-scale Modeling and Online Monitoring of Resin Flow through Dual-Scale Textiles in Liquid Composite Molding Processes. *Int. J. Adv. Manuf. Technol.* 96, 2215–2230. doi:10.1007/s00170-018-1703-9

Castro, J., Sket, F., and González, C. (2020). S-XCT Experimental Determination of Local Contact Angle and Meniscus Shape in Liquid Moulding of Composites. *Composites Sci. Techn.* 199, 108362. doi:10.1016/j.compscitech.2020.108362

Castro, J., Sket, F., Helfen, L., and González, C. (2021). *In Situ* local Imaging and Analysis of Impregnation during Liquid Moulding of Composite Materials Using Synchrotron Radiation Computed Laminography. *Composites Sci. Techn.* 215, 108999. doi:10.1016/j.compscitech.2021.108999

Causse, P., Ravey, C., and Trochu, F. (2018). Capillary Characterization of Fibrous Reinforcement and Optimization of Injection Strategy in Resin Transfer Molding. *J. Compos. Sci.* 2, 19. doi:10.3390/jcs2020019

Chai, B. X., Eisenbart, B., Nikzad, M., Fox, B., Blythe, A., Blanchard, P., et al. (2021). Simulation-based Optimisation for Injection Configuration Design of Liquid Composite Moulding Processes: A Review. *Composites Part A: Appl. Sci. Manufacturing* 149, 106540. doi:10.1016/j.compositesa.2021.106540

Chen, B., and Chou, T. W. (2000). Compaction of Woven-Fabric Preforms: Nesting and Multi-Layer Deformation. *Compos. Sci. Technol.* 60, 2223–2231. doi:10.1016/S0266-3538(00)00017-8

Chevalier, L., Bruchon, J., Moulin, N., Liotier, P.-J., and Drapier, S. (2018). Accounting for Local Capillary Effects in Two-phase Flows with Relaxed Surface Tension Formulation in Enriched Finite Elements. *Comptes Rendus Mécanique* 346, 617–633. doi:10.1016/j.crme.2018.06.008

Chiu, T.-H., Li, J.-B., Yao, Y., Wang, C.-W., Sun, S.-P., Hsu, C.-H., et al. (2018). Estimation of Local Permeability/porosity Ratio in Resin Transfer Molding. *J. Taiwan Inst. Chem. Eng.* 91, 32–37. doi:10.1016/j.jtice.2018.05.040

Chou, T.-W., Gao, L., Thostenson, E. T., Zhang, Z., and Byun, J.-H. (2010). An Assessment of the Science and Technology of Carbon Nanotube-Based Fibers and Composites. *Composites Sci. Techn.* 70, 1–19. doi:10.1016/j.compscitech.2009.10.004

Chung Hae Park, C. H., and Woo, L. (2011). Modeling Void Formation and Unsaturated Flow in Liquid Composite Molding Processes: A Survey and Review. *J. Reinforced Plastics Composites* 30, 957–977. doi:10.1177/0731684411411338

Cohades, A., Branfoot, C., Rae, S., Bond, I., and Michaud, V. (2018). Progress in Self-Healing Fiber-Reinforced Polymer Composites. *Adv. Mater. Inter.* 5, 1800177. doi:10.1557/mrs2008.16410.1002/admi.201800177

Correia, N. C., Robitaille, F., Long, A. C., Rudd, C. D., Šimáček, P., and Advani, S. G. (2004). Use of Resin Transfer Molding Simulation to Predict Flow, Saturation, and Compaction in the VARTM Process. *J. Fluids Eng. Trans. ASME* 126, 210–215. doi:10.1115/1.1669032

Devalve, C., and Pitchumani, R. (2013). Simulation of Void Formation in Liquid Composite Molding Processes. *Composites Part A: Appl. Sci. Manufacturing* 51, 22–32. doi:10.1016/j.compositesa.2013.03.016

Di Fratta, C., Klunker, F., and Ermanni, P. (2013). A Methodology for Flow-Front Estimation in LCM Processes Based on Pressure Sensors. *Composites Part A: Appl. Sci. Manufacturing* 47, 1–11. doi:10.1016/j.compositesa.2012.11.008

Duchemin, B., Cazaux, G., Gomina, M., and Bréard, J. (2021). Temperature-dependence of the Static Contact Angle: A Transition State Theory Approach. *J. Colloid Interf. Sci.* 592, 215–226. doi:10.1016/j.jcis.2021.02.059

Endruweit, A., Glover, P., Head, K., and Long, A. C. (2011). Mapping of the Fluid Distribution in Impregnated Reinforcement Textiles Using Magnetic Resonance Imaging: Application and Discussion. *Composites Part A: Appl. Sci. Manufacturing* 42, 1369–1379. doi:10.1016/j.compositesa.2010.11.01210.1016/j.compositesa.2011.05.020

Facciotto, S., Simacek, P., Advani, S. G., and Middendorf, P. (2021). Modeling of Anisotropic Dual Scale Flow in RTM Using the Finite Elements Method. *Composites B: Eng.* 214, 108735. doi:10.1016/j.compositesb.2021.108735

Fisher, S. L., Holmes, D. J., Jørgensen, J. S., Gajjar, P., Behnsen, J., Lionheart, W. R. B., et al. (2019). Laminography in the Lab: Imaging Planar Objects Using a Conventional X-ray CT Scanner. *Meas. Sci. Technol.* 30, 035401. doi:10.1088/1361-6501/aafcae

Foley, M. E., and Gillespie, J. W. (2005). Modeling the Effect of Fiber Diameter and Fiber Bundle Count on Tow Impregnation during Liquid Molding Processes. *J. Compos. Mater.* 39, 1045–1065. doi:10.1177/0021998305048739

Francucci, G., Rodríguez, E. S., and Vázquez, A. (2010). Study of Saturated and Unsaturated Permeability in Natural Fiber Fabrics. *Composites Part A: Appl. Sci. Manufacturing* 41, 16–21. doi:10.1016/j.compositesa.2009.07.012

Freeze, R. A., and Cherry, J. A. (1979). *Groundwater.* Englewood Cliffs, NJ: Prentice Hall, Inc.

Futaba, D. N., Hata, K., Yamada, T., Hiraoka, T., Hayamizu, Y., Kakudate, Y., et al. (2006). Shape-engineerable and Highly Densely Packed Single-Walled Carbon Nanotubes and Their Application as Super-capacitor Electrodes. *Nat. Mater* 5, 987–994. doi:10.1038/nmat1782

Gao, H., Yu, B., Duan, Y., and Fang, Q. (2014). Fractal Analysis of Dimensionless Capillary Pressure Function. *Int. J. Heat Mass Transfer* 69, 26–33. doi:10.1016/j.ijheatmasstransfer.2013.10.006

Garat, W., Le Moigne, N., Corn, S., Beaugrand, J., and Bergeret, A. (2020). Swelling of Natural Fibre Bundles under Hygro- and Hydrothermal Conditions: Determination of Hydric Expansion Coefficients by Automated Laser Scanning. *Composites Part A: Appl. Sci. Manufacturing* 131, 105803. doi:10.1016/j.compositesa.2020.105803

García, E. J., Hart, A. J., Wardle, B. L., Slocum, A. H., García, E. J., Hart, A. J. J., et al. (2007). Fabrication of Composite Microstructures by Capillarity-Driven Wetting of Aligned Carbon Nanotubes with Polymers. *Nanotechnology* 18, 165602. doi:10.1088/0957-4484/18/16/165602

Garcia, E., Wardle, B., Johnhart, A., and Yamamoto, N. (2008). Fabrication and Multifunctional Properties of a Hybrid Laminate with Aligned Carbon Nanotubes Grown *In Situ*. *Composites Sci. Techn.* 68, 2034–2041. doi:10.1016/j.compscitech.2008.02.028

Gascón, L., García, J. A., LeBel, F., Ruiz, E., and Trochu, F. (2016). A Two-phase Flow Model to Simulate Mold Filling and Saturation in Resin Transfer Molding. *Int. J. Mater. Form.* 9, 229–239. doi:10.1007/s12289-015-1225-z

Gascón, L., García, J. A., Lebel, F., Ruiz, E., and Trochu, F. (2015). Numerical Prediction of Saturation in Dual Scale Fibrous Reinforcements during Liquid Composite Molding. *Composites Part A: Appl. Sci. Manufacturing* 77, 275–284. doi:10.1016/j.compositesa.2015.05.019

Godbole, M. G., Purandare, R., Harshe, R., Hood, A., Gururaja, S., Joshi, M., et al. (2019). Influence of Filament Distribution on Transverse Tow Permeability: Model Predictions and Experimental Validation. *Composites Part A: Appl. Sci. Manufacturing* 118, 150–161. doi:10.1016/j.compositesa.2018.12.024

Gomez, C., Salvatori, D., Caglar, B., Trigueira, R., Orange, G., and Michaud, V. (2021). Resin Transfer Molding of High-Fluidity Polyamide-6 with Modified Glass-Fabric Preforms. *Composites Part A: Appl. Sci. Manufacturing* 147, 106448. doi:10.1016/j.compositesa.2021.106448

Gourichon, B., Binetruy, C., and Krawczak, P. (2006). A New Numerical Procedure to Predict Dynamic Void Content in Liquid Composite Molding. *Composites Part A: Appl. Sci. Manufacturing* 37, 1961–1969. doi:10.1016/j.compositesa.2005.12.017

Gresil, M., Revol, V., Kitsianos, K., Kanderakis, G., Koulalis, I., Sauer, M.-O., et al. (2017). EVITA Project: Comparison between Traditional Non-destructive Techniques and Phase Contrast X-Ray Imaging Applied to Aerospace Carbon Fibre Reinforced Polymer. *Appl. Compos. Mater.* 24, 513–524. doi:10.1007/s10443-016-9540-1

Gueroult, S., Lebel-Lavacry, A., Park, C. H., Bizet, L., Saouab, A., and Bréard, J. (2014). Analytical Modeling Andin Situmeasurement of Void Formation in Liquid Composite Molding Processes. *Adv. Compos. Mater.* 23, 31–42. doi:10.1080/09243046.2013.862383

Hamdaoui, M., Fayala, F., and Nasrallah, S. B. (2007). Dynamics of Capillary Rise in Yarns: Influence of Fiber and Liquid Characteristics. *J. Appl. Polym. Sci.* 104, 3050–3056. doi:10.1002/app.25642

Han, N., Baran, I., Zanjani, J. S. M., Yuksel, O., An, L., and Akkerman, R. (2020). Experimental and Computational Analysis of the Polymerization Overheating in Thick glass/Elium Acrylic Thermoplastic Resin Composites. *Composites Part B: Eng.* 202, 108430. doi:10.1016/j.compositesb.2020.108430

Hansen, D., Bomholt, N., Jeppesen, J. C., and Simonsen, A. C. (2017). Contact Angle Goniometry on Single Micron-Scale Fibers for Composites. *Appl. Surf. Sci.* 392, 181–188. doi:10.1016/j.apsusc.2016.09.018

Hassanizadeh, S. M., and Gray, W. G. (1990). Mechanics and Thermodynamics of Multiphase Flow in Porous media Including Interphase Boundaries. *Adv. Water Resour.* 13, 169–186. doi:10.1016/0309-1708(90)90040-B

He, Y., Li, Y., Hao, X., zhou, J., and Liu, S. (2019). Micro-flow Sensor for Continuous Resin Fluidity Monitoring between Fibers. *Sensors Actuators B: Chem.* 282, 177–186. doi:10.1016/j.snb.2018.11.022

Helfen, L., Myagotin, A., Mikulík, P., Pernot, P., Voropaev, A., Elyyan, M., et al. (2011). On the Implementation of Computed Laminography Using Synchrotron Radiation. *Rev. Scientific Instr.* 82, 063702. doi:10.1063/1.3596566

Helmig, R., Weiss, A., and Wohlmuth, B. I. (2007). Dynamic Capillary Effects in Heterogeneous Porous media. *Comput. Geosci.* 11, 261–274. doi:10.1007/s10596-007-9050-1

Hemmer, J., Burtin, C., Comas-Cardona, S., Binetruy, C., Savart, T., and Babeau, A. (2018). Unloading during the Infusion Process: Direct Measurement of the Dual-Scale Fibrous Microstructure Evolution with X-ray Computed Tomography. *Composites Part A: Appl. Sci. Manufacturing* 115, 147–156. doi:10.1016/j.compositesa.2018.09.013

Ho, K. K. C., Shamsuddin, S. R., Riaz, S., Lamorinere, S., Tran, M. Q., Javaid, A., et al. (2011). Wet Impregnation as Route to Unidirectional Carbon Fibre Reinforced Thermoplastic Composites Manufacturing. *Plastics, Rubber and Composites* 40, 100–107. doi:10.1179/174328911X12988622801098

Imbert, M., Comas-Cardona, S., Abisset-Chavanne, E., and Prono, D. (2018). Experimental Investigation of Intra-tow Fluid Storage Mechanisms in Dual-Scale Fiber Reinforcements. *Composites Part A: Appl. Sci. Manufacturing* 107, 70–82. doi:10.1016/j.compositesa.2017.12.015

Irfan, M., Harris, D., Paget, M., Ma, T., Leek, C., Machavaram, V., et al. (2021). On-site Evaluation of a Modified Pultrusion Process: Fibre Spreading and Resin Injection-Based Impregnation. *J. Compos. Mater.* 55, 77–93. doi:10.1177/0021998320943268

Irfan, M. S., Shotton-Gale, N., Paget, M. A., Machavaram, V. R., Leek, C., Wootton, S., et al. (2017). A Modified Pultrusion Process. *J. Compos. Mater.* 51, 1925–1941. doi:10.1177/0021998316666653

Kang, M., Lee, W. Il., and Hahn, H. T. (2000). Formation of Microvoids during Resin-Transfer Molding Process. *Compos. Sci. Technol.* 60, 2427–2434. doi:10.1016/S0266-3538(00)00036-1

Karbhari, V. M., and Palmese, G. R. (1997). Sizing Related Kinetic and Flow Considerations in the Resin Infusion of Composites. *J. Mater. Sci.* 32, 5761–5774. doi:10.1023/A:1018626002895

Kedari, V. R., Farah, B. I., and Hsiao, K.-T. (2011). Effects of Vacuum Pressure, Inlet Pressure, and Mold Temperature on the Void Content, Volume Fraction of Polyester/e-Glass Fiber Composites Manufactured with

VARTM Process. *J. Compos. Mater.* 45, 2727–2742. doi:10.1177/0021998311415442

Kessler, M. R., Sottos, N. R., and White, S. R. (2003). Self-healing Structural Composite Materials. *Composites Part A: Appl. Sci. Manufacturing* 34, 743–753. doi:10.1016/S1359-835X(03)00138-6

Kim, S. H., Jung, J. W., Li, M. X., Choi, S. W., Lee, W. I., and Park, C. H. (2017). Unsaturated Flow Behavior in Double-Scale Porous Reinforcement for Liquid Composite Molding Processes. *J. Reinforced Plastics Composites* 36, 85–97. doi:10.1177/0731684416671422

Konstantopoulos, S., Fauster, E., and Schledjewski, R. (2014). Monitoring the Production of FRP Composites: A Review of In-Line Sensing Methods. *Express Polym. Lett.* 8, 823–840. doi:10.3144/expresspolymlett.2014.84

Konstantopoulos, S., Grössing, H., Hergan, P., Weninger, M., and Schledjewski, R. (2018). Determination of the Unsaturated Through-Thickness Permeability of Fibrous Preforms Based on Flow Front Detection by Ultrasound. *Polym. Compos.* 39, 360–367. doi:10.1002/pc.23944

Kostornov, A. G., Moroz, A. L., Shapoval, A. A., Kabov, O., Strizhak, P., and Legros, J. C. (2015). Composite Structures with Gradient of Permeability to Be Used in Heat Pipes under Microgravity. *Acta Astronautica* 115, 52–57. doi:10.1016/j.actaastro.2015.04.022

Koubaa, S., Burtin, C., and Le Corre, S. (2016). Investigation of Capillary Impregnation for Permeability Prediction of Fibrous Reinforcements. *J. Compos. Mater.* 50, 1417–1429. doi:10.1177/0021998315593797

Labat, L., Bréard, J., Pillut-Lesavre, S., and Bouquet, G. (2001a). Void Fraction Prevision in LCM Parts. *Eur. Phys. J. AP* 16, 157–164. doi:10.1051/epjap:2001104

Labat, L., Grisel, M., Breard, J., and Bouquet, G. (2001b). Original Use of Electrical Conductivity for Void Detection Due to Injection Conditions of Composite Materials. *Comptes Rendus de l'Académie des Sci. - Ser. IIB - Mech.* 329, 529–534. doi:10.1016/S1620-7742(01)01363-0

Larson, N. M., Cuellar, C., and Zok, F. W. (2019). X-ray Computed Tomography of Microstructure Evolution during Matrix Impregnation and Curing in Unidirectional Fiber Beds. *Composites Part A: Appl. Sci. Manufacturing* 117, 243–259. doi:10.1016/j.compositesa.2018.11.021

Larson, N. M., and Zok, F. W. (2018). Insights from *In-Situ* X-ray Computed Tomography during Axial Impregnation of Unidirectional Fiber Beds. *Composites Part A: Appl. Sci. Manufacturing* 107, 124–134. doi:10.1016/j.compositesa.2017.12.024

Lawrence, J. M., Neacsu, V., and Advani, S. G. (2009). Modeling the Impact of Capillary Pressure and Air Entrapment on Fiber Tow Saturation during Resin Infusion in LCM. *Composites Part A: Appl. Sci. Manufacturing* 40, 1053–1064. doi:10.1016/j.compositesa.2009.04.013

Lebel, F., Fanaei, A. E., Ruiz, É., and Trochu, F. (2013). Experimental Characterization by Fluorescence of Capillary Flows in Dual-Scale Engineering Fabrics. *Textile Res. J.* 83, 1634–1659. doi:10.1177/0040517512471742

LeBel, F., Fanaei, A. E., Ruiz, É., and Trochu, F. (2014). Prediction of Optimal Flow Front Velocity to Minimize Void Formation in Dual Scale Fibrous Reinforcements. *Int. J. Mater. Form.* 7, 93–116. doi:10.1007/s12289-012-1111-x

LeBel, F., Ruiz, É., and Trochu, F. (2017). Experimental Study of Saturation by Visible Light Transmission in Dual-Scale Fibrous Reinforcements during Composite Manufacturing. *J. Reinforced Plastics Composites* 36, 1693–1711. doi:10.1177/0731684417725187

LeBel, F., Ruiz, É., and Trochu, F. (2019). Void Content Analysis and Processing Issues to Minimize Defects in Liquid Composite Molding. *Polym. Compos.* 40, 109–120. doi:10.1002/pc.24609

Leclerc, J. S., and Ruiz, E. (2008). Porosity Reduction Using Optimized Flow Velocity in Resin Transfer Molding. *Composites Part A: Appl. Sci. Manufacturing* 39, 1859–1868. doi:10.1016/j.compositesa.2008.09.008

Lee, J., Kessler, S. S., and Wardle, B. L. (2020). Void-Free Layered Polymeric Architectures via Capillary-Action of Nanoporous Films. *Adv. Mater. Inter.* 7, 1901427. doi:10.1002/admi.201901427

Léger, A., Molina-Jordá, J. M., Weber, L., and Mortensen, A. (2014). Percolation and Universal Scaling in Composite Infiltration Processing. *Mater. Res. Lett.* 3, 7–15. doi:10.1080/21663831.2014.948692

Léger, A., Weber, L., and Mortensen, A. (2015). Influence of the Wetting Angle on Capillary Forces in Pressure Infiltration. *Acta Materialia* 91, 57–69. doi:10.1016/j.actamat.2015.03.002

Leisen, J., and Beckham, H. W. (2008). Void Structure in Textiles by Nuclear Magnetic Resonance, Part I. Imaging of Imbibed Fluids and Image Analysis by Calculation of Fluid Density Autocorrelation Functions. *J. Textile Inst.* 99, 243–251. doi:10.1080/00405000701404122

Li, C., Cantarel, A., and Gong, X. (2020). A Study on Resin Infusion and Effects of Reinforcement Structure at Dual Scales by a Quasi-Realistic Numerical Simulation Method. *J. Compos. Mater.* 54, 4157–4171. doi:10.1177/0021998320926707

Li, M., Wang, S.-K., Gu, Y.-Z., Li, Y.-X., Potter, K., and Zhang, Z.-G. (2012). Evaluation of Through-Thickness Permeability and the Capillary Effect in Vacuum Assisted Liquid Molding Process. *Composites Sci. Techn.* 72, 873–878. doi:10.1016/j.compscitech.2012.02.014

Li, M., Wang, S., Gu, Y., Zhang, Z., Li, Y., and Potter, K. (2010). Dynamic Capillary Impact on Longitudinal Micro-flow in Vacuum Assisted Impregnation and the Unsaturated Permeability of Inner Fiber Tows. *Composites Sci. Techn.* 70, 1628–1636. doi:10.1016/j.compscitech.2010.06.004

Little, J. E., Yuan, X., and Jones, M. I. (2012). Characterisation of Voids in Fibre Reinforced Composite Materials. *NDT E Int.* 46, 122–127. doi:10.1016/j.ndteint.2011.11.011

Liu, H., Zhai, J., and Jiang, L. (2006). Wetting and Anti-wetting on Aligned Carbon Nanotube Films. *Soft Matter* 2, 811–821. doi:10.1039/b606654b

Liu, Y., Moulin, N., Bruchon, J., Liotier, P.-J., and Drapier, S. (2016). Towards Void Formation and Permeability Predictions in LCM Processes: A Computational Bifluid-Solid Mechanics Framework Dealing with Capillarity and Wetting Issues. *Comptes Rendus Mécanique* 344, 236–250. doi:10.1016/j.crme.2016.02.004

Louis, B. M., Maldonado, J., Klunker, F., and Ermanni, P. (2014). "Measurement of Nanoparticle Distribution in Composite Laminates Produced by Resin Transfer Molding," in 16th European Conference on Composite Materials ECCM 2014, Seville, Spain, June 22–26, 2014, 22–26.

Louis, B. M., Maldonado, J., Klunker, F., and Ermanni, P. (2019). Particle Distribution from In-Plane Resin Flow in a Resin Transfer Molding Process. *Polym. Eng. Sci.* 59, 22–34. doi:10.1002/pen.24860

Lu, J. G., Lee, S. B., Lundström, T. S., and Hwang, W. R. (2022). Numerical Simulation on Void Formation and Migration Using Stokes-Brinkman Coupling with Effective Dual-Scale Fibrous Porous media. *Composites Part A: Appl. Sci. Manufacturing* 152, 106683. doi:10.1016/j.compositesa.2021.106683

Lugo, J., Simacek, P., and Advani, S. G. (2014). Analytic Method to Estimate Multiple Equivalent Permeability Components from a Single Rectilinear experiment in Liquid Composite Molding Processes. *Composites Part A: Appl. Sci. Manufacturing* 67, 157–170. doi:10.1016/j.compositesa.2014.08.031

Lundström, T. S., and Gebart, B. R. (1994). Influence from Process Parameters on Void Formation in Resin Transfer Molding. *Polym. Compos.* 15, 25–33. doi:10.1002/pc.750150105

Lundström, T. S., Gebart, B. R., and Lundemo, C. Y. (1993). Void Formation in RTM. *J. Reinforced Plastics Composites* 12, 1339–1349. doi:10.1177/073168449301201207

Lundström, T. S., Stenberg, R., Bergström, R., Partanen, H., and Birkeland, P. A. (2000). In-plane Permeability Measurements: a Nordic Round-Robin Study. *Composites Part A: Appl. Sci. Manufacturing* 31, 29–43. doi:10.1016/S1359-835X(99)00058-5

Lystrup, C., George, A., Zobell, B., Boster, K., Childs, C., Girod, H., et al. (2021). Optical Measurement of Voids *In Situ* during Infusion of Carbon Reinforcements. *J. Compos. Mater.* 55, 775–786. doi:10.1177/0021998320959820

Madra, A., Hajj, N. E., and Benzeggagh, M. (2014). X-ray Microtomography Applications for Quantitative and Qualitative Analysis of Porosity in Woven Glass Fiber Reinforced Thermoplastic. *Composites Sci. Techn.* 95, 50–58. doi:10.1016/j.compscitech.2014.02.009

Manfredi, E., and Michaud, V. (2014). Packing and Permeability Properties of E-Glass Fibre Reinforcement Functionalised with Capsules for Self-Healing Applications. *Composites Part A: Appl. Sci. Manufacturing* 66, 94–102. doi:10.1016/j.compositesa.2014.07.006

Mantle, M. D., Bijeljic, B., Sederman, A. J., and Gladden, L. F. (2001). MRI Velocimetry and Lattice-Boltzmann Simulations of Viscous Flow of a Newtonian Liquid through a Dual Porosity Fibre Array. *Magn. Reson. Imaging* 19, 527–529. doi:10.1016/S0730-725X(01)00285-5

Matsuzaki, R., Kobayashi, S., Todoroki, A., and Mizutani, Y. (2013). Flow Control by Progressive Forecasting Using Numerical Simulation during Vacuum-Assisted Resin Transfer Molding. *Composites Part A: Appl. Sci. Manufacturing* 45, 79–87. doi:10.1016/j.compositesa.2012.09.014

Matsuzaki, R., Seto, D., Todoroki, A., and Mizutani, Y. (2014). Void Formation in Geometry-Anisotropic Woven Fabrics in Resin Transfer Molding. *Adv. Compos. Mater.* 23, 99–114. doi:10.1080/09243046.2013.832829

Matuzaki, R., Seto, D., Naito, M., Todoroki, A., and Mizutani, Y. (2015). Analytical Prediction of Void Formation in Geometrically Anisotropic Woven Fabrics during Resin Transfer Molding. *Composites Sci. Techn.* 107, 154–161. doi:10.1016/j.compscitech.2014.12.013

Mehdikhani, M., Gorbatikh, L., Verpoest, I., and Lomov, S. V. (2019). Voids in Fiber-Reinforced Polymer Composites: A Review on Their Formation, Characteristics, and Effects on Mechanical Performance. *J. Compos. Mater.* 53, 1579–1669. doi:10.1177/0021998318772152

Melelli, A., Arnould, O., Beaugrand, J., and Bourmaud, A. (2020). The Middle Lamella of Plant Fibers Used as Composite Reinforcement: Investigation by Atomic Force Microscopy. *Molecules* 25, 632. doi:10.3390/molecules25030632

Michaud, V. (2016). A Review of Non-saturated Resin Flow in Liquid Composite Moulding Processes. *Transp Porous Med.* 115, 581–601. doi:10.1007/s11242-016-0629-7

Michaud, V. J., Compton, L. M., and Mortensen, A. (1994). Capillarity in Isothermal Infiltration of Alumina Fiber Preforms with Aluminum. *Mmta* 25, 2145–2152. doi:10.1007/bf02652315

Michaud, V. (2021). "Permeability Properties of Composite Reinforcements," in *Composite Reinforcements for Optimum Performance* (Sawston: Woodhead Publishing). Editor P. Boisse. Second Edition, 443–472. doi:10.1016/B978-0-12-819005-0.00014-9

Mittal, G., Rhee, K. Y., Mišković-Stanković, V., and Hui, D. (2018). Reinforcements in Multi-Scale Polymer Composites: Processing, Properties, and Applications. *Composites Part B: Eng.* 138, 122–139. doi:10.1016/j.compositesb.2017.11.028

Morent, R., De Geyter, N., Verschuren, J., De Clerck, K., Kiekens, P., and Leys, C. (2008). Non-thermal Plasma Treatment of Textiles. *Surf. Coat. Techn.* 202, 3427–3449. doi:10.1016/j.surfcoat.2007.12.027

Mortensen, A., and Cornie, J. A. (1987). On the Infiltration of Metal Matrix Composites. *Mta* 18, 1160–1163. doi:10.1007/BF02668570

Mortensen, A., and Wong, T. (1990). Infiltration of Fibrous Preforms by a Pure Metal: Part III. Capillary Phenomena. *Mta* 21, 2257–2263. doi:10.1007/BF02647888

Moudood, A., Rahman, A., Öchsner, A., Islam, M., and Francucci, G. (2019). Flax Fiber and its Composites: An Overview of Water and Moisture Absorption Impact on Their Performance. *J. Reinforced Plastics Composites* 38, 323–339. doi:10.1177/0731684418818893

Mualem, Y. (1978). Hydraulic Conductivity of Unsaturated Porous media: Generalized Macroscopic Approach. *Water Resour. Res.* 14, 325–334. doi:10.1029/WR014i002p00325

Murray, J. J., Robert, C., Gleich, K., McCarthy, E. D., and Ó Brádaigh, C. M. (2020). Manufacturing of Unidirectional Stitched Glass Fabric Reinforced Polyamide 6 by Thermoplastic Resin Transfer Moulding. *Mater. Des.* 189, 108512. doi:10.1016/j.matdes.2020.108512

Neacsu, V., Abu Obaid, A., and Advani, S. G. (2006). Spontaneous Radial Capillary Impregnation across a Bank of Aligned Micro-cylinders - Part I: Theory and Model Development. *Int. J. Multiphase Flow* 32, 661–676. doi:10.1016/j.ijmultiphaseflow.2006.02.006

Neacsu, V., Leisen, J., Beckham, H. W., and Advani, S. G. (2007). Use of Magnetic Resonance Imaging to Visualize Impregnation across Aligned Cylinders Due to Capillary Forces. *Exp. Fluids* 42, 425–440. doi:10.1007/s00348-007-0251-0

Nguyen, V. H., Lagardère, M., Park, C. H., and Panier, S. (2014). Permeability of Natural Fiber Reinforcement for Liquid Composite Molding Processes. *J. Mater. Sci.* 49, 6449–6458. doi:10.1007/s10853-014-8374-1

Nishioka, G. M. (1990). Interaction of Organosilanes with Glass Fibers. *J. Non-Crystalline Sol.* 120, 102–107. doi:10.1016/0022-3093(90)90195-r

Nordlund, M., and Michaud, V. (2012). Dynamic Saturation Curve Measurement for Resin Flow in Glass Fibre Reinforcement. *Composites Part A: Appl. Sci. Manufacturing* 43, 333–343. doi:10.1016/j.compositesa.2011.12.001

Obande, W., Ó Brádaigh, C. M., and Ray, D. (2021). Continuous Fibre-Reinforced Thermoplastic Acrylic-Matrix Composites Prepared by Liquid Resin Infusion -

A Review. *Composites Part B: Eng.* 215, 108771. doi:10.1016/j.compositesb.2021.108771

Palmese, G. R., and Karbhari, V. M. (1995). Effects of Sizings on Microscopic Flow in Resin Transfer Molding. *Polym. Compos.* 16, 313–318. doi:10.1201/9781003064886-310.1002/pc.750160408

Panfilov, M. (2000). in *Theory and Applications of Transport in Porous Media*. Editor T. N. S. Majid Hassanizadeh (Utrecht, Netherlands: Department of Earth Sciences, Utrecht University). Utrecht and Founding Springer Available at: doi:10.1007/978-3-319-72826-1

Pantaloni, D., Bourmaud, A., Baley, C., Clifford, M. J., Ramage, M. H., and Shah, D. U. (2020). A Review of Permeability and Flow Simulation for Liquid Composite Moulding of Plant Fibre Composites. *Materials* 13, 4811–4823. doi:10.3390/ma13214811

Pantaloni, D., Rudolph, A. L., Shah, D. U., Baley, C., and Bourmaud, A. (2021). Interfacial and Mechanical Characterisation of Biodegradable Polymer-Flax Fibre Composites. *Composites Sci. Techn.* 201, 108529. doi:10.1016/j.compscitech.2020.108529

Park, C. H., Lebel, A., Saouab, A., Bréard, J., and Lee, W. I. (2011). Modeling and Simulation of Voids and Saturation in Liquid Composite Molding Processes. *Composites Part A: Appl. Sci. Manufacturing* 42, 658–668. doi:10.1016/j.compositesa.2011.02.005

Patel, N., and Lee, L. J. (1995). Effects of Fiber Mat Architecture on Void Formation and Removal in Liquid Composite Molding. *Polym. Compos.Compos* 16, 386–399. doi:10.1002/pc.750160507

Patel, N., and Lee, L. J. (1996). Modeling of Void Formation and Removal in Liquid Composite Molding. Part I: Wettability Analysis. *Polym. Compos.* 17, 96–103. doi:10.1002/pc.10594

Patiño, I. D., and Nieto-Londoño, C. (2021). Boundary Element Techniques for Multiscale Filling Simulations in Dual-Scale Fibrous Reinforcements Using Two Lumped Approaches. *Comput. Mech.* 68, 1223–1266. Springer Berlin Heidelberg. doi:10.1007/s00466-021-02066-6

Patiño, I. D., Power, H., Nieto-Londoño, C., and Flórez, W. F. (2017). Stokes-Brinkman Formulation for Prediction of Void Formation in Dual-Scale Fibrous Reinforcements: a BEM/DR-BEM Simulation. *Comput. Mech.* 59, 555–577. doi:10.1007/s00466-016-1360-5

Patiño-Arcila, I. D., and Vanegas-Jaramillo, J. D. (2018). Modeling and Simulation of Filling in Dual-Scale Fibrous Reinforcements: State of the Art and New Methodology to Quantify the Sink Effect. *J. Compos. Mater.* 52, 1915–1946. doi:10.1177/0021998317734038

Pierce, R. S., and Falzon, B. G. (2017). Simulating Resin Infusion through Textile Reinforcement Materials for the Manufacture of Complex Composite Structures. *Engineering* 3, 596–607. doi:10.1016/J.ENG.2017.04.006

Pillai, K. M., and Advani, S. G. (1996). Wicking across a Fiber-Bank. *J. Colloid Interf. Sci.* 183, 100–110. doi:10.1006/jcis.1996.0522

Pillai, K. M. (2004). Modeling the Unsaturated Flow in Liquid Composite Molding Processes: A Review and Some Thoughts. *J. Compos. Mater.* 38, 2097–2118. doi:10.1177/0021998304045585

Porfiri, M., and Gupta, N. (2009). Effect of Volume Fraction and wall Thickness on the Elastic Properties of Hollow Particle Filled Composites. *Composites Part B: Eng.* 40, 166–173. doi:10.1016/j.compositesb.2008.09.002

Pouchias, A., Cunningham, P. R., Stein, J., and Kazilas, M. (2019). Development of a Flexible Dielectric Sensor for Flow Monitoring of the Liquid Resin Infusion Process. *Sensors* 19, 5292. doi:10.3390/s19235292

Pucci, M. F., Duchemin, B., Gomina, M., and Bréard, J. (2020). Dynamic Wetting of Molten Polymers on Cellulosic Substrates: Model Prediction for Total and Partial Wetting. *Front. Mater.* 7. doi:10.3389/fmats.2020.00143

Pucci, M. F., Liotier, P.-J., and Drapier, S. (2015a). Capillary Effects on Flax Fibers - Modification and Characterization of the Wetting Dynamics. *Composites Part A: Appl. Sci. Manufacturing* 77, 257–265. doi:10.1016/j.compositesa.2015.03.010

Pucci, M. F., Liotier, P.-J., and Drapier, S. (2015b). Capillary Wicking in a Fibrous Reinforcement - Orthotropic Issues to Determine the Capillary Pressure Components. *Composites Part A: Appl. Sci. Manufacturing* 77, 133–141. doi:10.1016/j.compositesa.2015.05.031

Pucci, M. F., Liotier, P.-J., and Drapier, S. (2016). Capillary Wicking in Flax Fabrics - Effects of Swelling in Water. *Colloids Surf. A: Physicochemical Eng. Aspects* 498, 176–184. doi:10.1016/j.colsurfa.2016.03.050

Pucci, M. F., Liotier, P.-J., and Drapier, S. (2017a). Tensiometric Method to Reliably Assess Wetting Properties of Single Fibers with Resins: Validation on Cellulosic Reinforcements for Composites. *Colloids Surf. A: Physicochemical Eng. Aspects* 512, 26–33. doi:10.1016/j.colsurfa.2016.09.047

Pucci, M. F., Liotier, P.-J., Seveno, D., Fuentes, C., Van Vuure, A., and Drapier, S. (2017b). Wetting and Swelling Property Modifications of Elementary Flax Fibres and Their Effects on the Liquid Composite Molding Process. *Composites Part A: Appl. Sci. Manufacturing* 97, 31–40. doi:10.1016/j.compositesa.2017.02.028

Qian, H., Bismarck, A., Greenhalgh, E. S., and Shaffer, M. S. P. (2010a). Carbon Nanotube Grafted Silica Fibres: Characterising the Interface at the Single Fibre Level. *Composites Sci. Techn.* 70, 393–399. doi:10.1016/j.compscitech.2009.11.014

Qian, H., Greenhalgh, E. S., Shaffer, M. S. P., and Bismarck, A. (2010b). Carbon Nanotube-Based Hierarchical Composites: A Review. *J. Mater. Chem.* 20, 4751–4762. doi:10.1039/c000041h

Ravey, C., Ruiz, E., and Trochu, F. (2014). Determination of the Optimal Impregnation Velocity in Resin Transfer Molding by Capillary Rise Experiments and Infrared Thermography. *Composites Sci. Techn.* 99, 96–102. doi:10.1016/j.compscitech.2014.05.019

Reia Da Costa, E. F., Skordos, A. A., Partridge, I. K., and Rezai, A. (2012). RTM Processing and Electrical Performance of Carbon Nanotube Modified Epoxy/fibre Composites. *Composites Part A: Appl. Sci. Manufacturing* 43, 593–602. doi:10.1016/j.compositesa.2011.12.019

Rieser, J. M., Arratia, P. E., Yodh, A. G., Gollub, J. P., and Durian, D. J. (2015). Tunable Capillary-Induced Attraction between Vertical Cylinders. *Langmuir* 31, 2421–2429. doi:10.1021/la5046139

Rijswijk, K. v., Teuwen, J. J. E., Bersee, H. E. N., and Beukers, A. (2009). Textile Fiber-Reinforced Anionic Polyamide-6 Composites. Part I: The Vacuum Infusion Process. *Composites Part A: Appl. Sci. Manufacturing* 40, 1–10. doi:10.1016/j.compositesa.2008.03.018

Rougier, V., Cellier, J., Gomina, M., and Bréard, J. (2021). Slip Transition in Dynamic Wetting for a Generalized Navier Boundary Condition. *J. Colloid Interf. Sci.* 583, 448–458. doi:10.1016/j.jcis.2020.09.015

Ruiz, E., Achim, V., Soukane, S., Trochu, F., and Bréard, J. (2006). Optimization of Injection Flow Rate to Minimize Micro/macro-Voids Formation in Resin Transfer Molded Composites. *Composites Sci. Techn.* 66, 475–486. doi:10.1016/j.compscitech.2005.06.013

Sahimi, M. (2011). *Flow and Transport in Porous Media and Fractured Rock: From Classical Methods to Modern Approaches*. 2nd ed. Weinheim, Germany: Wiley VCH. doi:10.1002/9783527636693

Salokhe, S., Rahmati, M., and Masoodi, R. (2021). Numerical Modelling of the Flow in a Swelling Preform during LCM Mould Filling. *J. Reinforced Plastics Composites* 40, 490–504. doi:10.1177/0731684420975197

Salvatori, D., Caglar, B., and Michaud, V. (2019). 3D Spacers Enhance Flow Kinetics in Resin Transfer Molding with Woven Fabrics. *Composites Part A: Appl. Sci. Manufacturing* 119, 206–216. doi:10.1016/j.compositesa.2019.01.023

Salvatori, D., Caglar, B., Teixidó, H., and Michaud, V. (2018). Permeability and Capillary Effects in a Channel-wise Non-crimp Fabric. *Composites Part A: Appl. Sci. Manufacturing* 108, 41–52. doi:10.1016/j.compositesa.2018.02.015

Sas, H. S., Šimáček, P., and Advani, S. G. (2015). A Methodology to Reduce Variability during Vacuum Infusion with Optimized Design of Distribution media. *Composites Part A: Appl. Sci. Manufacturing* 78, 223–233. doi:10.1016/j.compositesa.2015.08.011

Schell, J. S. U., Deleglise, M., Binetruy, C., Krawczak, P., and Ermanni, P. (2007). Numerical Prediction and Experimental Characterisation of Meso-Scale-Voids in Liquid Composite Moulding. *Composites Part A: Appl. Sci. Manufacturing* 38, 2460–2470. doi:10.1016/j.compositesa.2007.08.005

Schmachtenberg, E., Schulte Zur Heide, J., and Töpker, J. (2005). Application of Ultrasonics for the Process Control of Resin Transfer Moulding (RTM). *Polym. Test.* 24, 330–338. doi:10.1016/j.polymertesting.2004.11.002

Schneider, G., Weber, L., and Mortensen, A. (2019). Reactive Pressure Infiltration of Cu-46at.Pct. Si into Carbon. *Acta Materialia* 177, 9–19. doi:10.1016/j.actamat.2019.07.010

Sharma, S., Siginer, D. A., Dukipatti, R. K., and Soschinske, K. A. (2009). Effect of Fiber Sizing - Test Fluid Interaction on the Unsaturated and Saturated Flow in the VARTM Process. *J. Compos. Mater.* 43, 1589–1601. doi:10.1177/0021998308337898

Simacek, P., and Advani, S. G. (2003). A Numerical Model to Predict Fiber Tow Saturation during Liquid Composite Molding. *Composites Sci. Techn.* 63, 1725–1736. doi:10.1016/S0266-3538(03)00155-6

Simacek, P., Neacsu, V., and Advani, S. G. (2010). A Phenomenological Model for Fiber Tow Saturation of Dual Scale Fabrics in Liquid Composite Molding. *Polym. Compos.* 31, 1881–1889. doi:10.1002/pc.20982

Sinha, E., and Panigrahi, S. (2009). Effect of Plasma Treatment on Structure, Wettability of Jute Fiber and Flexural Strength of its Composite. *J. Compos. Mater.* 43, 1791–1802. doi:10.1177/0021998309338078

Sisodia, S. M., Garcea, S. C., George, A. R., Fullwood, D. T., Spearing, S. M., and Gamstedt, E. K. (2016). High-resolution Computed Tomography in Resin Infused Woven Carbon Fibre Composites with Voids. *Composites Sci. Techn.* 131, 12–21. doi:10.1016/j.compscitech.2016.05.010

Spitalsky, Z., Tasis, D., Papagelis, K., and Galiotis, C. (2010). Carbon Nanotube-Polymer Composites: Chemistry, Processing, Mechanical and Electrical Properties. *Prog. Polym. Sci.* 35, 357–401. doi:10.1016/j.progpolymsci.2009.09.003

Staal, J., Caglar, B., Hank, T., Wardle, B. L., Gorbatikh, L., Lomov, S. V., et al. (2021). In-series Sample Methodology for Permeability Characterization Demonstrated on Carbon Nanotube-Grafted Alumina Textiles. *Composites Part A: Appl. Sci. Manufacturing* 150, 106631. doi:10.1016/j.compositesa.2021.106631

Steenkamer, D. A., McKnight, S. H., Wilkins, D. J., and Karbhari, V. M. (1995). Experimental Characterization of Permeability and Fibre Wetting for Liquid Moulding. *J. Mater. Sci.* 30, 3207–3215. doi:10.1007/BF01209239

Stöven, T., Weyrauch, F., Mitschang, P., and Neitzel, M. (2003). Continuous Monitoring of Three-Dimensional Resin Flow through a Fibre Preform. *Composites Part A: Appl. Sci. Manufacturing* 34, 475–480. doi:10.1016/S1359-835X(03)00059-9

Strauß, S., Senz, A., and Ellinger, J. (2019). Comparison of the Processing of Epoxy Resins in Pultrusion with Open bath Impregnation and Closed-Injection Pultrusion. *J. Compos. Sci.* 3, 87. doi:10.3390/jcs3030087

Studer, J., Dransfeld, C., Jauregui Cano, J., Keller, A., Wink, M., Masania, K., et al. (2019). Effect of Fabric Architecture, Compaction and Permeability on through Thickness Thermoplastic Melt Impregnation. *Composites Part A: Appl. Sci. Manufacturing* 122, 45–53. doi:10.1016/j.compositesa.2019.04.008

Tan, H., and Pillai, K. M. (2012). Multiscale Modeling of Unsaturated Flow in Dual-Scale Fiber Preforms of Liquid Composite Molding I: Isothermal Flows. *Composites Part A: Appl. Sci. Manufacturing* 43, 1–13. doi:10.1016/j.compositesa.2010.12.013

Tanner, L. H. (1979). The Spreading of Silicone Oil Drops on Horizontal Surfaces. *J. Phys.-D.* 12, 1473–1484. doi:10.1088/0022-3727/12/9/009

Teixidó, H., Caglar, B., Revol, V., and Michaud, V. (2021). In-operando Dynamic Visualization of Flow through Porous Preforms Based on X-ray Phase Contrast Imaging. *Composites Part A: Appl. Sci. Manufacturing* 149, 106560. doi:10.1016/j.compositesa.2021.106560

Testoni, G. A., Kim, S., Pisupati, A., and Park, C. H. (2018). Modeling of the Capillary Wicking of Flax Fibers by Considering the Effects of Fiber Swelling and Liquid Absorption. *J. Colloid Interf. Sci.* 525, 166–176. doi:10.1016/j.jcis.2018.04.064

Thomas, S., Bongiovanni, C., and Nutt, S. R. (2008). *In Situ* estimation of Through-Thickness Resin Flow Using Ultrasound. *Composites Sci. Techn.* 68, 3093–3098. doi:10.1016/j.compscitech.2008.07.012

Thomason, J. L. (2021). "Sizing Chemistry of Glass Fibers," in *Fiberglass Science and Technology* (Switzerland AG, Cham: Springer Nature). Editor H. Li, 259–321. doi:10.1007/978-3-030-72200-510.1007/978-3-030-72200-5_4

Thostenson, E. T., Li, W. Z., Wang, D. Z., Ren, Z. F., and Chou, T. W. (2002). Carbon Nanotube/carbon Fiber Hybrid Multiscale Composites. *J. Appl. Phys.* 91, 6034–6037. doi:10.1063/1.1466880

van Genuchten, M. T. (1980). A Closed-form Equation for Predicting the Hydraulic Conductivity of Unsaturated Soils. *Soil Sci. Soc. America J.* 44, 892–898. doi:10.2136/sssaj1980.03615995004400050002x

Varnavides, G., Mortensen, A., and Carter, W. C. (2021). Simulating Infiltration as a Sequence of Pinning and De-pinning Processes. *Acta Materialia* 210, 116831. doi:10.1016/j.actamat.2021.116831

Vedernikov, A., Safonov, A., Tucci, F., Carlone, P., and Akhatov, I. (2020). Pultruded Materials and Structures: A Review. *J. Compos. Mater.* 54, 4081–4117. doi:10.1177/0021998320922894

Vernet, N., Ruiz, E., Advani, S., Alms, J. B., Aubert, M., Barburski, M., et al. (2014). Experimental Determination of the Permeability of Engineering Textiles: Benchmark II. *Composites Part A: Appl. Sci. Manufacturing* 61, 172–184. doi:10.1016/j.compositesa.2014.02.010

Verrey, J., Michaud, V., and Månson, J.-A. E. (2006). Dynamic Capillary Effects in Liquid Composite Moulding with Non-crimp Fabrics. *Composites Part A: Appl. Sci. Manufacturing* 37, 92–102. doi:10.1016/j.compositesa.2005.04.011

Vilà, J., Sket, F., Wilde, F., Requena, G., González, C., and LLorca, J. (2015). An *In Situ* Investigation of Microscopic Infusion and Void Transport during Vacuum-Assisted Infiltration by Means of X-ray Computed Tomography. *Composites Sci. Techn.* 119, 12–19. doi:10.1016/j.compscitech.2015.09.016

Villière, M., Guéroult, S., Sobotka, V., Boyard, N., Bréard, J., and Delaunay, D. (2015). Dynamic Saturation Curve Measurement in Liquid Composite Molding by Heat Transfer Analysis. *Composites Part A: Appl. Sci. Manufacturing* 69, 255–265. doi:10.1016/j.compositesa.2014.11.024

Vo, H. N., Pucci, M. F., Corn, S., Le Moigne, N., Garat, W., Drapier, S., et al. (2020). Capillary Wicking in Bio-Based Reinforcements Undergoing Swelling - Dual Scale Consideration of Porous Medium. *Composites Part A: Appl. Sci. Manufacturing* 134, 105893. doi:10.1016/j.compositesa.2020.105893

Walther, J., Simacek, P., and Advani, S. G. (2012). The Effect of Fabric and Fiber Tow Shear on Dual Scale Flow and Fiber Bundle Saturation during Liquid Molding of Textile Composites. *Int. J. Mater. Form.* 5, 83–97. doi:10.1007/s12289-011-1060-9

Wang, B. C., Huang, Y. D., and Liu, L. (2006). Effects of Fibre Surface Silanisation on Silica Fibre/phenolics Composites Produced by Resin Transfer Moulding Process. *Mater. Sci. Techn.* 22, 206–212. doi:10.1179/174328406X91078

Wang, J., Fuentes, C. A., Zhang, D., Wang, X., Van Vuure, A. W., and Seveno, D. (2017a). Wettability of Carbon Fibres at Micro- and Mesoscales. *Carbon* 120, 438–446. doi:10.1016/j.carbon.2017.05.055

Wang, J., Simacek, P., and Advani, S. G. (2016). Use of Centroidal Voronoi Diagram to Find Optimal Gate Locations to Minimize Mold Filling Time in Resin Transfer Molding. *Composites Part A: Appl. Sci. Manufacturing* 87, 243–255. doi:10.1016/j.compositesa.2016.04.026

Wang, J., Simacek, P., and Advani, S. G. (2017b). Use of Medial axis to Find Optimal Channel Designs to Reduce Mold Filling Time in Resin Transfer Molding. *Composites Part A: Appl. Sci. Manufacturing* 95, 161–172. doi:10.1016/j.compositesa.2017.01.003

Wang, Y., Moatamedi, M., and Grove, S. M. (2009). Continuum Dual-Scale Modeling of Liquid Composite Molding Processes. *J. Reinforced Plastics Composites* 28, 1469–1484. doi:10.1177/0731684408089533

Washburn, E. W. (1921). Note on a Method of Determining the Distribution of Pore Sizes in a Porous Material. *Proc. Natl. Acad. Sci.* 7, 115–116. doi:10.1073/pnas.7.4.115

Wei, M., Bowman, R. S., Wilson, J. L., and Morrow, N. R. (1993). Wetting Properties and Stability of Silane-Treated Glass Exposed to Water, Air, and Oil. *J. Colloid Interf. Sci.* 157, 154–159. doi:10.1006/jcis.1993.1170

Willenbacher, B., May, D., and Mitschang, P. (2019). Out-of-plane Capillary Pressure of Technical Textiles. *Composites Part A: Appl. Sci. Manufacturing* 124, 105495. doi:10.1016/j.compositesa.2019.105495

Withers, P. J., Bouman, C., Carmignato, S., Cnudde, V., Grimaldi, D., Hagen, C. K., et al. (2021). X-ray Computed Tomography. *Nat. Rev. Methods Primers* 1, R29–R43. doi:10.1038/s43586-021-00015-4

Wolfrath, J., Michaud, V., Modaressi, A., and Månson, J.-A. E. (2006). Unsaturated Flow in Compressible Fibre Preforms. *Composites Part A: Appl. Sci. Manufacturing* 37, 881–889. doi:10.1016/j.compositesa.2005.01.008

Wu, D., and Larsson, R. (2020). A Shell Model for Resin Flow and Preform Deformation in Thin-Walled Composite Manufacturing Processes. *Int. J. Mater. Form.* 13, 923–937. doi:10.1007/s12289-019-01517-z

Wu, X.-F., and Dzenis, Y. A. (2006). Droplet on a Fiber: Geometrical Shape and Contact Angle. *Acta Mechanica* 185, 215–225. doi:10.1007/s00707-006-0349-0

Yamamoto, N., Wicks, S. S., Guzman, R., Ishiguro, K., and Steiner, S. A. (2009). "Mechanical, Thermal, and Electrical Properties of Woven Laminated Advanced Composites Containing Aligned Carbon Nanotubes," in ICCM: 17th Conference on Composite Materials, Edinburgh, United Kingdom, July 27–31, 2009.

Yashiro, S., Nakashima, D., Oya, Y., Okabe, T., and Matsuzaki, R. (2019). Particle Simulation of Dual-Scale Flow in Resin Transfer Molding for Process Analysis.

Composites Part A: Appl. Sci. Manufacturing 121, 283–288. doi:10.1016/j. compositesa.2019.03.038

Yeager, M., Hwang, W. R., and Advani, S. G. (2016). Prediction of Capillary Pressure for Resin Flow between Fibers. *Composites Sci. Techn.* 126, 130–138. doi:10.1016/j.compscitech.2016.02.014

Yeager, M., Simacek, P., and Advani, S. G. (2017). Role of Fiber Distribution and Air Evacuation Time on Capillary Driven Flow into Fiber Tows. *Composites Part A: Appl. Sci. Manufacturing* 93, 144–152. doi:10.1016/j.compositesa.2016.11.016

Yin, T., Li, Y., and Yuan, B. (2018). The Multi-Scale Flow Behaviors of Sisal Fiber Reinforced Composites during Resin Transfer Molding Process. *Sci. China Technol. Sci.* 61, 1925–1934. doi:10.1007/s11431-018-9343-5

Yoshihara, K., Kamei, Y., Mizuno, A., Ohgaki, H., Hori, T., and Ueno, I. (2020). Effect of Wettability on Viscous Fluid Impregnation in Single-Layer Woven-Fibre Bundles Driven by Pressure Difference. *Composites Part A: Appl. Sci. Manufacturing* 138, 106049. doi:10.1016/j.compositesa.2020.106049

Yousaf, Z., Potluri, P., and Withers, P. J. (2017). Influence of Tow Architecture on Compaction and Nesting in Textile Preforms. *Appl. Compos. Mater.* 24, 337–350. doi:10.1007/s10443-016-9554-8

Yum, S. H., Lee, W. I., and Kim, S. M. (2016). Particle Filtration and Distribution during the Liquid Composite Molding Process for Manufacturing Particles Containing Composite Materials. *Composites Part A: Appl. Sci. Manufacturing* 90, 330–339. doi:10.1016/j.compositesa.2016.07.016

Yun, M., Sas, H., Simacek, P., and Advani, S. G. (2017). Characterization of 3D Fabric Permeability with Skew Terms. *Composites Part A: Appl. Sci. Manufacturing* 97, 51–59. doi:10.1016/j.compositesa.2016.12.030

Zhang, H., Liu, Y., Huo, S., Briscoe, J., Tu, W., Picot, O. T., et al. (2017). Filtration Effects of Graphene Nanoplatelets in Resin Infusion Processes: Problems and Possible Solutions. *Composites Sci. Techn.* 139, 138–145. doi:10.1016/j. compscitech.2016.12.020

Zhang, X., Wang, P., Zhou, Y., Li, X., Yang, E.-H., Yu, T. X., et al. (2016). The Effect of Strain Rate and Filler Volume Fraction on the Mechanical Properties of Hollow Glass Microsphere Modified Polymer. *Composites Part B: Eng.* 101, 53–63. doi:10.1016/j.compositesb.2016.06.079

Zhao, C., Yang, B., Wang, S., Ma, C., Wang, S., and Bi, F. (2019). Three-Dimensional Numerical Simulation of Meso-Scale-Void Formation during the Mold-Filling Process of LCM. *Appl. Compos. Mater.* 26, 1121–1137. doi:10.1007/s10443-019-09770-w

Zingraff, L., Michaud, V., Bourban, P.-E., and Månson, J.-A. E. (2005). Resin Transfer Moulding of Anionically Polymerised Polyamide 12. *Composites Part A: Appl. Sci. Manufacturing* 36, 1675–1686. doi:10.1016/j.compositesa.2005.03.023